
# A theoretical study of dinitrogen activation and reduction by molybdenum porphyrins

Heiðar Már Aðalsteinsson

Faculty of Physical Sciences
University of Iceland
2016

# A THEORETICAL STUDY OF DINITROGEN ACTIVATION AND REDUCTION BY MOLYBDENUM PORPHYRINS

Heiðar Már Aðalsteinsson

15 ECTS thesis submitted in partial fulfillment of a
*Baccalaureus Scientiarum* degree in Chemistry

Advisor
Ragnar Björnsson

Co-advisor
Egill Skúlason

Faculty of Physical Sciences
School of Engineering and Natural Sciences
University of Iceland
Reykjavik, June 2016

A theoretical study of dinitrogen activation and reduction by molybdenum porphyrins
15 ECTS thesis submitted in partial fulfillment of a B.Sc. degree in Chemistry



Faculty of Physical Sciences
School of Engineering and Natural Sciences
University of Iceland
VRII, Hjarðarhagi 2-6
107, Reykjavik
Iceland

Telephone: 525 4000

Bibliographic information:
Heiðar Már Aðalsteinsson, 2016, A theoretical study of dinitrogen activation and reduction by molybdenum porphyrins, B.Sc. thesis, Faculty of Physical Sciences, University of Iceland.

Reykjavik, Iceland, June 2016

# Abstract

Interest in nitrogen fixation by molecular catalysts has steadily increased since reports of a successful catalytic conversion of dinitrogen to ammonia at ambient conditions a little over a decade ago. Currently, only a few molecular systems capable of catalytic dinitrogen reduction to ammonia have been reported, two of which are molybdenum based. This study explores dinitrogen activation, and reduction, with hypothetical molybdenum metalloporphyrin catalysts by means of quantum chemical calculations, in an attempt to combine the well documented redox properties of porphyrins with the ability of molybdenum to bind and activate dinitrogen.

A sensitivity to variations in axial ligands and peripheral porphyrin ring substitutions is reported, with regard to both binding and activation of dinitrogen. Strong sigma donors in the axial position increase activation, whilst inhibiting binding. Alternatively strong pi acceptors decrease activation as they compete with dinitrogen for electrons. Moderate sigma donors are predicted to achieve binding and considerable activation. Halogen axial ligands predicted the strongest dinitrogen activation. Sensitivity to modifications suggests the possibility of adjusting the catalyst to obtain desirable properties.

Calculations of the entire reaction pathway revealed a competing pathway towards hydrazine formation, which was energetically favorable with fluoride as the axial ligand, and very close in energy using acetonitrile. Moreover, the calculations were performed with two functionals showing great variations in results, indicating the need for a benchmarking study to establish a trustworthy protocol.

# Útdráttur

Áhugi á sameindahvataðri afoxun tvíniturs til að mynda ammóníak hefur stöðugt aukist síðan sýna tókst fram á að það væri yfir höfuð mögulegt fyrir rúmum áratugi síðan. Einungis fáir hvatar sem færir eru um slíka efnahvötun hafa verið smíðaðir, þar af tveir sem innihalda molybdenum. Porfýrín eru lífvirk efni með mjög fjölbreytta virkni, og þekkt fyrir þáttöku sína í mörgum oxunar- afoxunar efnahvörfum. Markmið þessarar rannsóknar var að kanna getu ýmissa molybdenum málmporfýrína til að virkja og afoxa tvínitur, reist á þeirri tilgátu að þekkt oxunarafoxunar hæfni porfýrína ásamt getu molybdenum til að binda og afoxa nitur, gætu leitt til öflugra efnahvata fyrir slík hvörf.

Breyting áslægra tengla, sem og breyting hópa á porfýrín hring, höfðu mikil áhrif á bæði bindingu- og virkjun tvíniturs. Sterkir sigma gjafar í áslægri stöðu leiddu til verri bindingar en meiri virkjunar tvíniturs, á meðan sterkir pí þegar leiddu til minni virkjunar vegna samkeppni við tvínitur um rafeindir. Besta útkoma m.t.t. bindingar og virkjunar var með mildum sigma gjöfum. Viðkvæmni kerfis fyrir breytingum bendir til þess að hægt sé að smíða hvata með eftirsóknarverðum eiginleikum með réttu vali á tenglum.

Reikningar á hvarfgangi leiddu í ljós að annar hvarfgangur sem leiðir til myndun hydrazine, er í samkeppni við þann sem leiðir til myndunar ammóníaks, og var sá hvarfgangur ýmist hagstæðari eða mjög líkur m.t.t. orku, eftir því hvaða tenglar voru notaðir.

# Contents

# List of Figures

# List of Tables

# Abbreviations

| | |
|---|---|
| Acn | - Acetonitrile |
| $Cp_2Cr'$ | - Decamethylchromocene (apostrophy for decamethyl) |
| depe | - 1.2-bis(diethylphosphino)ethane |
| DFT | - Density functional theory |
| dppe | - 1.2-bis(diphenylphosphino)ethane |
| EA | - Electron affinity |
| GGA | - Generalized gradient approximation |
| HF | - Hartree-Fock |
| HIPT | - Hexaisopropylterphenyl |
| HOMO | - Highest occupied molecular orbital |
| KS | - Kohn-Sham |
| L(S)DA | - Local (spin) density approximation |
| LUMO | - Lowest occupied molecular orbital |
| Lut | - Lutidine (conjugate base of $LutH^+$) |
| $LutH^+$ | - Lutidinium acid |
| MO | - Molecular orbital |
| NHC | - N-heterocyclic carbene |
| NPA | - Natural population analysis |
| OEP | - Octaethylporphyrin |
| PCN | - Pthalocyanine |
| PNP | - 2.6-bis(di-tertbutylphosphinomethyl)pyridine |
| $PMe_3$ | - Trimethylphosphine |
| Por | - Porphine |
| Py | - Pyridine |
| SCF | - Self consistent field method |
| TPP | - Tetraphenylporphyrin |

# Acknowledgments

I would like to thank Ragnar Björnsson, PhD, for excellent tutoring in the field of quantum and computational chemistry, as well as all the support in conducting this research and helping me write this thesis. I would also like to thank Egill Skúlason, PhD, for granting me the opportunity to work on his research team a year ago, and for taking the time to proofread this thesis. Additionally I thank Háskóli Íslands for allowing me to use their super computer clusters to conduct the research. I would like to thank my family for the support during my studies, especially my wife, without whom I probably could not have finished this project. Finally I would like to thank my friends and colleagues at Háskóli Íslands for the enjoyable times we had doing our research projects.

# 1. Introduction

## 1.1. Dinitrogen reduction and Mo complexes

Ammonia is one of the most produced chemicals in the world. World production estimated by the U.S annual geological survey is roughly 177 million metric tonnes, about 88% of which is used for fertilizer[1]. Currently, the most common way to reduce $N_2$ to $NH_3$ is the Haber-Bosch process, where stoichiometric amounts of dinitrogen and dihydrogen are heated under pressure in the presence of a catalyst[2]. This process is quite energy demanding, both from maintaining the high temperature and pressure during the reaction, as well as producing dihydrogen from natural gas (mostly methane) for the reaction, which is extremely energy demanding, on top of coming from a finite resource.

Nitrogenases, a group of similar enzymes found in certain types of bacteria, can, however, reduce $N_2$ to $NH_3$ at ambient conditions in solution with protons and electrons, yielding 2 equivalents of $NH_3$ and 1 of $H_2$. The process is, however, also energy demanding in organisms, as the enzyme uses 16 equivalents of ATP per equvalent of $N_2$[3]. The most studied, as well as most efficient nitrogenase is the molybdenum nitrogenase, yet less active ones with V or Fe instead of Mo exist[4]. Although these enzymes have been studied for decades and general understanding of them has increased greatly, especially over the last few years, the mechanism and pathway of nitrogen reduction has not yet been determined. However, it is known that the mechanism involves a stepwise process of protonations and electron additions (reductions)[5]. Furthermore, it was only recently that X-ray analysis revealed the complete structure of the active site of the enzyme called the FeMo cofactor[6,7]. Recent progress in the understanding of nitrogenase, coupled with Schrock's and Yandulov's first successful molecular catalyst for reduction of $N_2$ in 2003[8], has fueled interest within the scientific community of finding a suitable transition metal complex capable of activating and reducing $N_2$ to $NH_3$ efficiently. Many researchers are currently studying the subject.

The Schrock-Yandulov complex, which was first to achieve catalytic reduction of $N_2$ in 2003 was a $[(HIPTNCH_2CH_2)_3N]Mo(III)$ complex (figure 1.1a.), abbreviated $[HIPTN_3N]Mo$ where HIPT stands for hexa-iso-propyl-terphenyl, which is a bulky substituent on a triamidoamine ligand. The proton source used in the catalytic reaction was lutidinium 3,5-$B[(CF_3)_2C_6H_3]_4$, abbreviated $[LutH^+][BAr'_4]$, and the electron source was decamethylchromatocene ($Cp_2Cr'$). Originally, cobaltocene ($Cp_2Co$) was used as the reducing agent, with which they achieved systematic formation of many intermediates by varying reductant concentration. It was, however, not a strong enough reducing agent to achieve the final reduction step, resulting in the use of $Cp_2Cr'$ which is stronger by 0.2 V in acetonitrile, making its redox potential $E = 1.5$ V using a $Cp_2Fe/[Cp_2Fe]^+$ standard[9]. The reaction was carried out in heptane and yielded 63% $NH_3$ comparing to amount of reducing agent and acid used (36 and 48 eq), which in this case was 4 turover cycles, or just under 8 equivalents compared to Mo. Schrock *et al.* proposed a mechanism based on the 6 intermediates (revised to 8 in 2008[10]) they were able to isolate, with molybdenum going from oxidation state Mo(III) to Mo(VI) and back in a cycle of stepwise protonations and reductions, which has since been called the "Schrock cycle" (figure 1.2)[8]. The first step of the cycle remained ambiguous, but after a series of computational studies of the $[HIPTN_3N]Mo$ by various research groups, 3 different possibilities were proposed as the first step of the reaction. The first was a protonation of the $\beta$ (terminal) N atom of $N_2$ followed by an electron transfer, second was a reduction to $[(HIPTN_3N)MoN_2]^-$ followed by a protonation of the $\beta$ N atom, and the third was a "proton-catalyzed addition of an electron", which is when one of the amido N atoms (of the triamidoamine ligand) is protonated followed by a reduction of $N_2$ leading to a zwitterion, in which the proton migrates to $N_2$. Based on computational evidence from Reiher *et al.*[11,12], as well as his own experimental evidence for the amido protonated complex, Schrock considered the third one to be correct[10].

In the 1970's Chatt *et al.* studied bis(dinitrogen) complexes of Mo and W containing bidentate phosphine ligands (figure 1.1 b.1) with regard to $N_2$ reduction, and in doing so was one of the first researchers to study molecular catalytic reduction of $N_2$. Chatt suggested a catalytic cycle of stepwise protonations and reductions of an end-on coordinated $N_2$ to a single metal center, much like the Schrock cycle, apart from the metal cycling through oxitation states M(0) and M(III)[13,16]. However, none of the intermediates Chatt proposed had been characterized at the time. As a result, the Chatt cycle is not very well defined regarding the order of the protonation and reduction steps, and they may vary depending on the catalyst being used. For example, the lowest energy pathway for conversion of $N_2$ to $NH_3$ has been calculated for all complexes labeled b. in figure 1.1 by Tuczek *et al.*[17–19], none

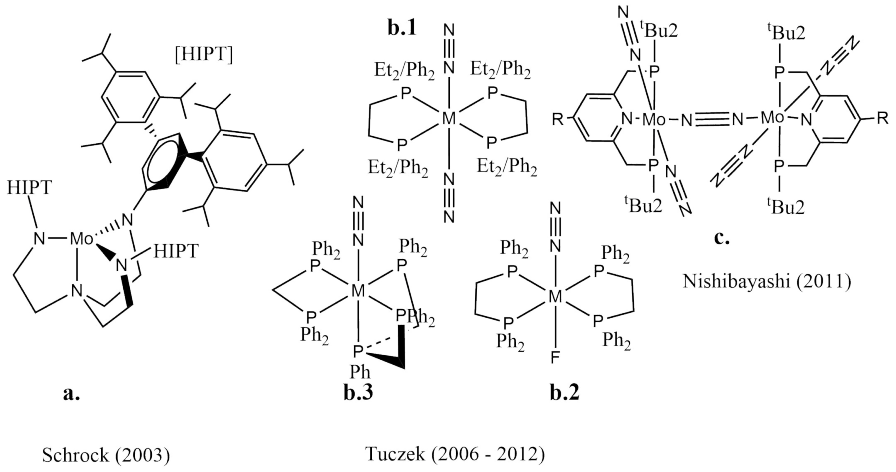


*Figure 1.1:* ***a.*** *The catalytically active [HIPTN$_3$N]Mo.* ***b.1, b.2:*** *Molybdenum/Tungsten complexes of bidentate phosphine ligands originally studied by Chatt et al.*[13]*, and later in more detail by Tuczek et al.(see text)*[14]*.* ***b.3*** *Another Mo(0) phosphine complex of dinitrogen where a tridentate phosphine ligand now occupies the trans position to the $N_2$ ligand, also studied by Tuczek et al..* ***c.*** *[Mo(N$_2$)$_2$(PNP)]$_2$($\mu$-N$_2$), a recently discovered PNP-pincer Mo dimer bridged with dinitrogen, synthesized and proven catalytically active by Nishibayashi et al.*[15]*.*

of which have the same order of steps. They did, however, characterize several of the intermediates spectroscopically and computationally[14], also showing that the metal oxidation states in the Chatt cycle varies between M(0) and M(IV), with the nitrido complex formed after release of the first $NH_3$ being M(IV). Figure 1.2 shows a general Chatt cycle of **b.1** as depicted in a recent review article[20], which differs slightly, regarding bond orders of intermediates, from the cycle suggested in 2006 by Tuczek *et al.*[17].

In 2006, Tuczek *et al.* carried out a spectroscopic and computational study on several dinitrogen complexes, where they correlated $N_2$ activation with calculated natural population analysis (NPA) charges of the N atoms and the vibrational frequency[17], where a lower NN vibrational frequency (weaker bond) and larger negative charge on the N atoms suggested greater $N_2$ activation. These parameters have since been commonly used to evaluate $N_2$ activation. Two of the systems they characterized were molybdenum complexes, one being the previously mentioned Schrock catalyst and the other [M(N$_2$)$_2$(depe/dppe)] (figure 1.1 **b.1**) (depe = 1,2-bis(diethylphosphino)ethane and dppe=1,2-bis(diphenyl-phosphino)ethane), Mo(0) and W(0) complexes. The complexes were predicted to only moderately activate

$N_2$ based on the NPA charge analysis and NN vibrational frequency, which was consistent with existing experimental data[21]. A computational study focusing more on the mechanism and energetics, of the Chatt cycle (described below)[18], in which it was assumed that the axial ligand (an intermediate in **b.1** mechanism) would stay coordinated througout the cycle. Although the calculations seemed to indicate a thermally allowed catalytic cycle, they also showed a possibility for hydrazine formation in the cycle that would compete with $NH_3$ formation. Yet another problem with bidentate phosphine complexes, is that they undergo disproportionation, where the bis-dinitrogen complex and a difluoro complex are formed, resulting in a loss of 50% of catalyst every cycle. In order to avoid disproportionation, tridentate phosphine complexes, originally synthesized by Dahlenburg *et al.*[22], and tetradentate phosphine complexes of dinitrogen were synthesized and studied in an attempt to occupy the *trans* position of the $N_2$ ligand. They have been unable to demonstrate catalytic activity of these complexes as of yet.[19,20].

A recent success in molecular catalyzed $N_2$ reduction, is the dinitrogen briged molybdenum dimer complex, $[Mo(N_2)_2(PNP)]\ 2\,(\mu\text{-}N_2)$ (PNP = 2,6-bis(di-tert-butylphosphinomethyl)pyridine, often called PNP pincer ligands) (figure 1.1 c.), reported by Nishibayashi *et al.*[25,26]. It is still unclear whether the dimer or the monomer is the catalytically active species. The group originally reported catalytic activity of the PNP pincer complexes in 2010, but have since modified it with respect to the R-groups to achieve maximum efficiency and increase reaction rate. Inspired by the structure of nitrogenase enzymes and the interaction between iron and molybdenum in the FeMo cofactors, they decided to introduce ferrocene as R group on the pyridine rings. Ferrocene is also attractive because of its capability to undergo facile reversible one electron redox reactions. The reaction time was reduced significantly with ferrocene, and the yield was 45 equivalents of ammonia (22 per Mo atom) relative to the catalyst. Lutidinium was used as a proton source and the reaction carried out in toluene. Additionally, no unwanted side products, such as hydrazine, were reported.

Complexes of metals other than molybdenum have also been studied thoroughly, with iron being the other predominant metal used in molecular catalyzed $N_2$ reduction, and the only successful example being the iron dinitrogen complexes reported by Peters *et al.*[27]. The complex is anionic, containing a tetradentate tris(phosphine)borane ligand. The reaction was performed in diethylether using $KC_8$ as a reducing agent and Brookhart's acid as the proton source at $-78°C$. The yield was 7 equivalents relative to the catalyst, and 44% relative to the proton source. The low temperature is needed to avoid dihydrogen formation. No products of side reactions were reported. The group has studied several iron complexes

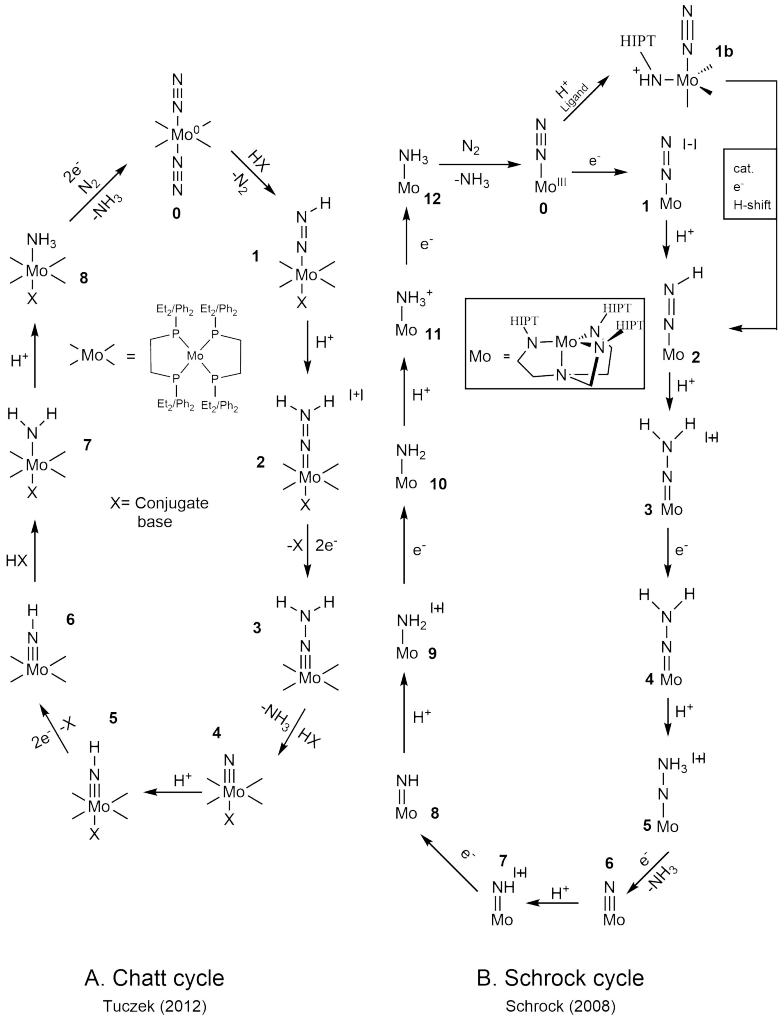


*Figure 1.2:* ***A.*** *A general representation of the Chatt cycle as portrayed by Tuczek et al. in 2012[20]. The cycle varies slightly in bond order from the one they reported in 2006[17]. The hydrazido complex* ***(2)*** *had a single N-N bond and the reduced complex thereafter* ***(3)*** *had a double M-N bond as well as the reduced imido complex* ***(6)****.* ***B****. The Schrock complex as reported by Schrock in 2008. The alternative first step was suggested by Schrock, although it is usually shown as a strictly alternating protonation and reduction steps starting with a protonation[23,24]*

regarding $N_2$ reduction, some of which have Si or C replacing the borane in the complex described above, but none have been as successful as the iron borane complex.

## 1.2. Metalloporphyrins

Metalloporphyrins are highly versatile molecules with multiple functions. They are also photosensitive and electrochemically active, thus, show great promise in the development of new types photovoltaic cells[28]. Various biological processes depend on metalloporphyrins, such as reversable oxygen binding of hemoglobin, and the electron transferring of the heme group in cytochrome enzymes[29]. Interesting liquid crystalline materials (mesogens) have been synthesized from metalloporphyrins[30], and they are well known for their redox activity[31]. With techniques in synthesizing symmetrically and unsymmetrically substituted porphyrins improving greatly over the last few decades, almost any peripherally substituted porphyrin system can be synthesized, according to Vicente *et al.*[32]. Metals can bind to porphyrins in several different ways, there are examples of large metals bridging two porphyrin rings, bridging of two metalloporphyrins by other molecules, and metals lying out of the porphyrin plane, leading to unusual structures[33]. With that in mind, considering the flora of available axial ligands, all of which affects the chemistry of metalloporphyrins, their possible applications seem endless.

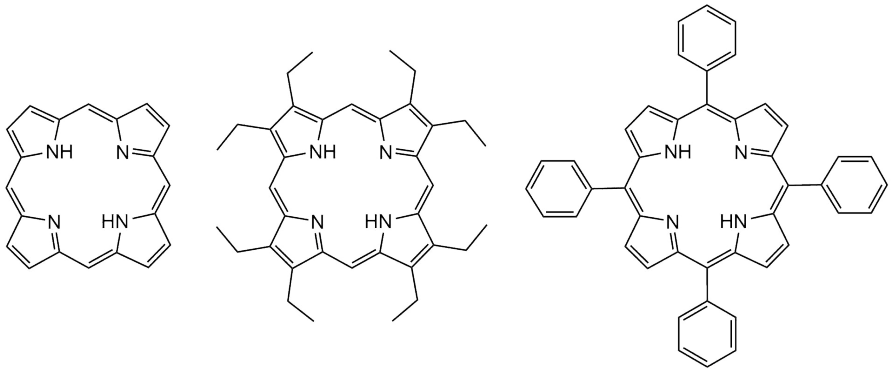


*Figure 1.3: Three common porphyrins, here in their uncoordinated neutral form* ***Left:*** *Porphine, the building block of porphyrins. Not commonly used without having peripheral substituents as the others, can even be asymmetrically substituted.* ***Mid:*** *Octaethylporphyrin, commonly abbreviated OEP.* ***Right*** *Tetraphenylporphyrin, commonly abbreviated TPP*

The simplest porphyrin, porphine, consists of four cyclicly 2,5 bound pyrrole rings with one $sp^2$ carbon between them and the N atoms facing the center, making it a macrocycle of conjugated $\pi$ electrons with the N atoms forming a suitable binding site for metals in the center (figure 1.3). Upon ligation the porphyrin generally gets deprotonated, making it a di-ionic tetradentate ligand. The large delocalized pi electron system surrounding a central metal atom may allow for

charge transfer between the two, as porphyrins are known to commonly part-take in intra-molecular electron transfers, contributing to their high redox activity[34].

High valent molybdenum complexes of Mo(V) and Mo(VI) have been reported, all of them, however, have oxo or peroxo ligands to balance the charge, and would therefore unlikely bind $N_2$[33]. Mo(IV) complexes exist as 5-coordinate and 6-coordinate species. The 5-coordinate complexes usually contain multiply bonded oxo or nitrito ligands, although they have also been synthesized with sulfido and seleno ligands[35]. The 6-coordinate Mo(IV) complexes exists with various axial ligands, for example two chlorides or chloride and phenyl. The $[Mo(IV)(Por)Cl_2]$ complex is an important intermediate in synthesizing Mo(II) porphyrins. Mo(II) porphyrins are the most relevant of porphinatomolybdenums in $N_2$ activation chemistry due to the low oxidation state. They have been reported with several neutral ligands including pyridine, carbonyl and diphenylacetylen. The pyridine ligands are *trans*, as would be expected, and the diphenylacetylen is $\eta^2$ coordinated in a pseudo square pyramidal conformation. What is unusal about the carbonyl ligand is that it is *cis*, and the complex is diamagnetic, which is unusual for a Mo(II) porphyrin with a $d^4$ configuration[33,36].

## 1.3. Aim of this study

This study explored activation and reduction of $N_2$ to $NH_3$ on hypothetical, low-valent porphinatomolybdenum complexes by quantum chemical calculations. The delocalized $\pi$ electron system of porphyrins, and their well documented redox activity combined with the ability of molybdenum to bind and reduce $N_2$ were hypothesized to be complementary properties for the design of a molecular catalyst, capable of reducing $N_2$.

Primary steps of a proposed reaction mechanism were calculated for various porphyrin complexes with systematic alterations of the axial ligands used, as well as peripheral substitutions of the porphyrin ring. Activation of $N_2$ was evaluated using the first protonation energy as a measurement, as it is the most endothermic step in most calculations relating to molecular $N_2$ reduction. Vibrational frequencies of N-N bonds and atomic charges of the N atoms were also evaluated, as they have been proposed as benchmarks for $N_2$ activation.

Promising candidates were then chosen for calculations of a complete pathway of Gibbs free reaction enthalpies towards formation of $NH_3$, using porphinatomolybdenum as a porphyrin model. Results were then compared to calculations of the Chatt and Schrock systems.

# 2. Theory

## 2.1. Hartree-Fock theory

When performing quantum chemistry calculations, one is essentially trying to solve the Schroedinger equation for a molecular or solid system to determine the ground state (or possibly excited states) electronic structure and the corresponding energy. Such calculations, if accurate, may be used for predictions about chemical reactions and properties of the system. Unfortunately we cannot solve the Schroedinger equation for many particles due to their interdependency, i.e. electrons do not move independently of one another, thus many approximations must be involved. This chapter covers a brief description of the principles used in computational chemistry, especially pertaining to this research, but a detailed description of quantum mechanics is outside the scope of this text.

$$\hat{H}\Psi(r,R) = E\Psi(r,R) \tag{2.1}$$

$$\hat{H} = \hat{T}_N(R) + \hat{T}_e(r) + V_{eN} + V_{NN} + V_{ee}$$

$$\hat{H}_{elec}\Psi_{elec}(r,R) = E_{elec}\Psi_{elec}(r,R) \tag{2.2}$$

$$\hat{H} = \hat{T}_e(r) + V_{eN} + V_{NN} + V_{ee}$$

Equation 2.1 is the most general form of the time-independent Schroedinger equation where the wavefunction $\Psi$ is a function of all nuclei (R) and electrons (r) of the system and the T-terms of the Hamiltonian are kinetic energies of nuclei and electrons, and the V-terms are the following Coulomb interactions: electron-nucleus, nucleus-nucleus and electron-electron[37]. Equation 2.2 is the electronic Schroedinger equation, accompanied by the electronic Hamiltonian. They are derived from the Born-Oppenheimer approximation, which states that the energies of the nuclei and electrons can be calculated separately, essentially simplifying the Schroedinger equation by removing the term $\hat{T}_N$, although it still needs to be cal-

culated as a separate problem. Hartree proposed a model where electrons in an atom moved independently of each other and the multi-electron wave function $\Psi_{elec}$ could be sepatated into a product of independent single-electron wave functions[38], $\phi_i(r)$, called orbitals. The kinetic energy could then be calculated as a sum of the energies from the single electron wave functions (Hartree kinetic functional). This model was shortly thereafter expanded to include molecules, by delocalizing $\phi_i(r)$ making them molecular orbitals (MO).

$$E_T^{H28} = -\frac{1}{2}\sum_i^N \int \phi(r)\nabla^2\phi(r)dr \tag{2.3}$$

Fock later showed that Hartree's wave function was in violation of the Pauli exclusion principle because it was not antisymmetric[39]. He proposed a modification, which made the wave function antisymmetric and all terms of electron self-interaction canceled out (Fock exchange functional). This form of $\Psi_{elec}$ can be written as a Slater determinant (proposed later by Slater)[40]. Equation 2.4 shows a Slater determinant of N electrons and equation 2.5 shows the Fock exchange functional. It should be noted that every orbital in equation 2.4 is a product of a spatial orbital ($\phi_i(r)$) and a spin function $\alpha(\omega)$ (up) or $\beta(\omega)$ (down), i.e. a spin orbital.

$$\Psi_{elec}(x_1,\dots x_N) = \frac{1}{\sqrt{N!}}\begin{vmatrix} \phi_1(x_1) & \phi_2(x_1) & \dots & \phi_N(x_1) \\ \phi_1(x_2) & \phi_2(x_2) & \dots & \dots \\ \vdots & \vdots & & \dots \\ \phi_1(x_N) & \phi_2(x_N) & \dots & \phi_N(x_N) \end{vmatrix} \tag{2.4}$$

$$E_X^{F30} = -\frac{1}{2}\sum_i^N\sum_j^N \int\int \frac{\phi_i^*\phi_j\phi_j^*\phi_i}{r_{12}} \tag{2.5}$$

In modern computational chemistry, these orbitals are a linear combination of basis functions($\sum_i c_i\kappa_i$), and the basis functions themselves are a linear combination of known functions, most commonly Gaussian functions. Many collections of basis functions, called basis sets, have been created. These collections vary in size, and their size is usually denoted by $\zeta$. For example, a triple-$\zeta$ basis set, uses three basis functions to describe each valence orbital (electron) of every atom in the system.

$$E_0 \leq \frac{\int \Psi^*_{trial} \hat{H} \Psi_{trial} d\tau}{\int \Psi^*_{trial} \Psi_{trial} d\tau} \tag{2.6}$$

The variational principle (equation 2.6) shows that any trial wave function will have greater or equal energy than the ground state. Hence, larger basis sets that improve the wave function will get closer to the ground state energy, although within limits of Hartree-Fock (HF) theory. The HF energy can be derived from inserting the Slater determinant into the variational equation and minimizing with respect to the MO coefficients, $c_i$. This is a more complicated task than it seems, and yields equations 2.7 and 2.8.

The first term of equation 2.7 is the Hartree kinetic functional and with an added term for nuclear electron attraction, $\hat{T}_e(r) + V_{eN}$ in the Hamiltonian of 2.1. The other two terms are two electron integrals, called Coulomb and exchange integrals. The exchange integral [ij|ji] is the exchange functional in 2.5, which does not describe a real interaction but rather arises from making the wave function antisymmetric. The Coulomb integral is similar, except the orbitals i and j are paired, and it describes Coulomb repulsions between the electrons.

$$E_{HF} = \sum_i^N \langle i | \, \hat{h} \, | i \rangle + \frac{1}{2} \sum_{i,j}^N [ii|jj] - [ij|ji] \tag{2.7}$$

$$\hat{F} = \hat{h}_i + \sum_j^N (\hat{J}_{ij} - \hat{K}_{ij})$$

$$\hat{F}\phi_i = \epsilon_i \phi_i \tag{2.8}$$

Minimizing equation 2.7 with respect to the MO coefficients yields N eigenvalue problems 2.8. These are called the HF equations, where $\hat{F}$ is the Fock operator and the eigenvalue $\epsilon_i$ is the energy of orbital i. The first term of the Fock operator is the same as in 2.7, but the second one is a slightly different integral derived from the Coulomb and Exchange integrals which, when summed, gives an average potential, $V^{eff}$, from all electrons. The much simpler $V^{eff}$ replaces the $V_{ee}$ term in the Schroedinger equation. Using the Gaussian-based orbitals from before and matrix calculations, not discussed here, the HF eigenvalue equations can be solved. As the orbitals appear on both sides of the equation, they can be calculated with the self consistent field method (SCF), starting with an initial guess

and the output used iteratively until the energy stops changing. Finally adding the separately calculated $\hat{T}_N$ term for nuclear kinetic energy (usually solved computationally by harmonic frequency calculations), all terms in the 2.1 Hamiltonian are then accounted for.

HF theory is far from perfect. It does not account for any correlation energy (see next section) or instantaneous electron interactions, the Hartree kinetic functional assumes no electron interactions, and Slater determinants are not perfect approximations for wave functions. Many post HF methods exist that greatly improve the HF wave function, by including combinations of excited state slater determinants, but they will not be discussed here. Instead we move to another approach called density functional theory (DFT).

## 2.2. Density functional theory

Before beginning the discussion on density functional theory, it is useful to divide the total electronic energy of the system into the 5 terms of equation 2.9[41], which is just a different formulation of the electronic Schroedinger equation 2.2. $E_T$ and $E_V$ are the kinetic energy of electrons and coulomb interactions between electrons and nuclei. $E_J$ is the Coulomb energy of an independently moving electron that also interacts with(repels) it self. $E_X$, the exchange functional, mainly corrects the problem of electron self interaction and $E_C$, the correlation energy, mainly accounts for the correlated movement of electrons. The equations that the terms consist of are called functionals, functions that use functions instead of numbers as arguments. Relating it to the HF theory, $E_T + E_V$ are in the first term of the Fock operator (Hartree kinetic functional eq.2.3), $E_J$ is the Coulomb integrals, and $E_X$ the exchange integrals (Fock exhcange functional eq.2.5). The HF method does not include correlation energy, $E_C$.

$$E_{elec} = E_T + E_V + E_J + E_X + E_C \tag{2.9}$$

In 1927, Thomas and Fermi conceived the first kinetic functional that was only dependent on electron density, $\rho$, which was based on a model of uniform electron gas, sometimes called jellium[42,43]. This was remarkable for two reasons, the first being that kinetic energy is not electrostatic and being able to calculate it from electron density is surprising to say the least. Secondly, the wave function has

3 spatial variables for every particle in the system, whereas the electron density is a function of a total of 3 spatial variables, meaning that calculations of large systems would be simplified to a great extent. A few years later Dirac made an exact exchange functional for jellium[44], $E_X^{D30}$. Since then, density functionals for each of the terms in equation 2.9 have been derived, although many of them not very accurate. Hohenberg and Kohn not only proved that all of the information in equation 2.9 can be expressed in terms of electron density, but also that it is exact if the correct functionals are used. Unfortunately, we still do not know what these functionals are, or what they should look like[45].

Slater originally proposed mixing of HF functionals and density functionals in 1951, when he suggested simplifying the HF energy equation by replacing the Fock exchange functional with Diracs's $E_X^{D30}$[46]. Years later, Kohn and Sham proved that DFT was still exact in principle if orbital-based HF kinetic functionals were used to calculate the kinetic energy, $E_T$, and density functionals used for exchange and correlation energy, $E_X + E_C$, commonly expressed as a single exchange-correlation functional $E_{XC}$[47]. This type of DFT has since been called Kohn Sham (KS) DFT, and is usually what is being referred to when DFT is mentioned, as it is by far the most common type of DFT currently employed. The problem remaining is the $E_{XC}$ functional, which would need to correct everything inexact in the equations, most likely leading to an extremely complex functional.

Density functionals for $E_{XC}$ can be separated into several classes. A class that is not so commonly used anymore due to inaccurate results is the local density approximation (LDA), or local spin density approximation for open shell systems (LSDA). Kinetic energy is calculated with the Hartree kinetic functional, but replacing the Fock exchange functional with Dirac's $E_X^{D30}$ exchange, and, originally, the VWN correlation functional, both of which were designed to calculate the uniform electron gas[41], but other correlation functionals have been used as well. The generalized gradient approximation (GGA) takes inhomogeneity of the electron density into account by adding gradient corrections, and is thus considered an improvement to L(S)DA methods, as electron density is far from uniform in molecules. A common GGA exchange functional is the Becke 88 ( $E_X^{B88}$) functional[48]. It has been used in combination with various correlation functionals, such as the Lee-Yang-Parr correlation, called BLYP when combined, or the Perdew 86 correlation functional, then called BP86. Yet another common type of functionals are hybrid functionals. These employ a linear combination of HF exchange and DFT exchange where the coefficients are fitted from experimental data, the most common one probably being B3LYP. Equations 2.10 - 2.12 show the composition of the Becke 88, BP86 and B3LYP functionals.

$$E^{BP86} = E_T^{H28} + E_V + E_J + E_X^{B88} + E_C^{PW91} \tag{2.10}$$

$$E^{B88} = E_X^{D30} - b \int \rho_\alpha^{4/3} \frac{x_\alpha^2}{1 + 6\beta x_\alpha sinh^{-1} x_\alpha} \tag{2.11}$$

$$\begin{aligned} E^{B3LYP} &= E_T^{H28} + E_V + E_J + (1 - c1)E_X^{D30} + c1E_X^{F30} + c2E_X^{B88} \\ &+ (1 - c3)E_c^{VWN} + c3E_C^{LYP} \end{aligned} \tag{2.12}$$

The KS equations are very similar to the HF equations when it comes to calculating minimum energy due to the use of the $E_T^{H28}$ functional, which uses orbitals and Slater wave functions. A set of eigenvalue problems is obtained, with the main difference being that the Fock exchange terms have been replaced by density-based exchange-correlation functionals, $v_{XC}[\rho(r)]$, in the Kohn Sham operator in equation 2.13.

$$F^{KS}[\rho(r)] = h_i[\rho(r)] + \sum_j^{max} J_{ij}[\rho(r)] + v_{XC}[\rho(r)] \tag{2.13}$$

Geometry optimizations of all molecules in this study were performed with the BP86 functional and def2-SVP double $\zeta$ basis sets for atoms C and H. The larger def2-TZVP triple $\zeta$ basis set was used for all other atoms in the calculations[49]. The RI-J approximation was used with the def2-SVP/J auxiliary basis set[50]. The D3BJ van der Waals correction by Grimme was used in all calculations[51], as was the COSMO continuum solvation model[52], with solvent dielectric constant set to acetonitrile. Harmonic frequency calculations were used to confirm minima and saddle points, as well as obtaining thermal, entropic and zero point energy corrections. Single point energy calculations were performed on optimized geometries with the B3LYP hybrid functional and def2-TZVP basis sets for all atoms. The RIJCOSX approximation using def2-TZVP/J auxiliary basis sets[53], D3BJ correction and COSMO continuum solvation model were all used in the single point calculations. All calculations were performed with ORCA 3.0.3.[54]

# 3. Results and discussion

## 3.1. Electronic structure

Redox reactions are any reactions in which the oxidation states of the reactants are altered. Many such reactions, including the molecular catalyzed reduction of $N_2$, involve direct electron transfer steps. To that end, it is useful to understand the electronic structure of a potential catalyst, and, additionally, to see how modifications to the catalyst affect its electron affinity, as the complex needs to receive six electrons to achieve formation of 2 equivalents of $NH_3$ . The energy required to reduce several Mo(II) porphyrins (porphines) by two electrons was calculated to evaluate the effects of different axial ligands on electron affinities (EA) of the Mo(Por) complexes. The results can be seen in table 3.1. Metallocenes have been used experimentally in the catalytic reduction of $N_2$ [8,25], making cobaltocene a reasonable option to use as a reference in the calculations, and thus, all reduction steps include the energy of $Cp_2Co \longrightarrow [Cp_2Co]^+$. The first part of the table shows complexes of dinitrogen with different *trans*-axial ligands and, in the second half shows the reduction energies of complexes containing the same axial ligand at both sites.

Strong $\pi$ acceptors, such as the $N_2$ and CO ligands, increase the EA, as seen by the highly exergonic first electron reduction. This is contrasts the findings of Scheiner *et al.* [55], who reported the opposite effect calculated for Fe(II) and Co(II) porphyrins when coordinating to CO ligands. This is, however, not necessarily a contradictory result, as Fe(II) and Co(II) have 2 and 3 additional d-electrons. The EA decreases with increasing $\sigma - donor$ strength (for poor $\pi$ acceptors), with the first reduction energy approaching zero for Acn. and Py., and becoming endergonic for $NH_3$, and the stronger donors, $PMe_3$ and NHC. Interestingly, in the upper part of table 3.1 where one ligand is fixed as $N_2$, the first electron transfer is always exergonic, suggesting that having only one $\pi$ acceptor ligand makes the complex susceptible to reduction. Moreover, the second reduction was much less endergonic in the in the presence of $N_2$, which was not the case for CO, suggesting

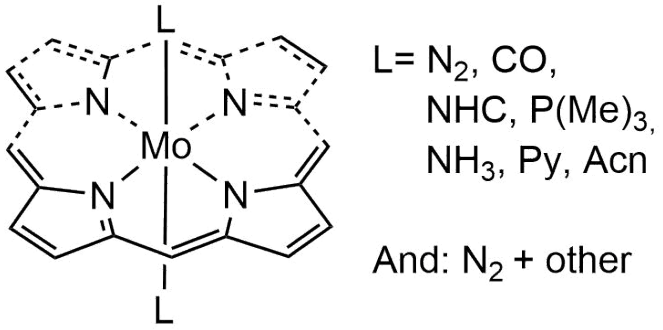


*Figure 3.1: Porphinatomolybdenum with two axial ligands. The list shows ligands used in the calculation of a 2 $e^-$ reduction. Calculations were made where L was the same ligand, and where one L was fixed as $N_2$ while others varied. The planar porphinatomolybdenum was also calculated.*

some favorable interaction between the complex and $N_2$ rather than an effect of coordinated $\pi$ acceptors. Changes in spin state were noteworthy as well. All complexes containing axial ligands went from a triplet to a doublet state after the first reduction step, as would be expected based on $\mathrm{Mo(II)\,S=1 \longrightarrow Mo(I)\,S=\frac{1}{2}}$. After adding a second electron the spin state reverted to a triplet state, indicating participation of porphine orbitals. Furthermore the quintet state of the planar porphinatomolybdenum suggested participation of the $d_{z^2}$ orbital, which should be lowered substantially in the absence of axial ligands.

In order to gain better insight into the results in table 3.1, and determine the oxidation state of the metal, especially after the second reduction step, electronic structures of selected complexes were analyzed by calculating and visualizing their respective MOs. We chose to analyze the neutral free base porphine ligand, the complexed square planar Mo(Por), and the six-coordinated bis(dinitrogen) and bis(trimethylphosphino) complexes. This allowed us to analyze the effect coordination to the metal has on the porphine orbitals, as well as comparing the different effects of strong $\sigma$ donor and $\pi$ acceptor axial ligands on porphine and metal orbitals. The results are shown in MO diagrams in figure 3.2. All data shown here comes from the canonical orbitals arising directly from the DFT equations, mentioned in a previous chapter.

The calculated HOMO-LUMO gap of the porphine molecule was 44.9 kcal/mol. The highest orbital included in figure 3.2, $b_{1u}$, down to the $a_{1u}$ orbital, match those reported by Scheiner *et al.*[55]. Their HOMO, however, was the $a_{1u}$ with the $a_{2u}$ as LUMO. While our calculations were of the protonated neutral porphine, theirs were of the deprotonated porphine, but the charge of their system was not men-

*Table 3.1: The energy of reduction in several [Mo(II)(Por)$X_2$] complexes with different axial ligands. All complexes are octahedrally coordinated with the exception of the first one being the square planar porphinatomolybdenum(II). The superscript on the left of each compound denotes the spin multiplicity. ("(Por)" has been omitted from equations in the case of axially ligated complexes for sake of table space ). Abbreviations are as follows, Acn = acetonitrile, NHC= N-heterocyclic carbene, Py = pyridine, $PMe_3$ = trimethylphosphine. M= Mo.*

| **First reduction** | $\Delta E$ kcal/mol | **Second reduction** | $\Delta E$ kcal/mol |
|---|---|---|---|
| $^5[M(Por)] + e^- \rightarrow {}^4[M(Por)]^-$ | −2.44 | $^4[M(Por)]^- + e^- \rightarrow {}^3[M(Por)]^{2-}$ | 9.90 |
| $^3[M(N_2)_2] + e^- \rightarrow {}^2[M(N_2)_2]^-$ | −18.3 | $^2[M(N_2)_2]^- + e^- \rightarrow {}^3[M(N_2)_2]^{2-}$ | 18.5 |
| $^3[M(N_2)(CO)] + e^- \rightarrow {}^2[M(N_2)(CO)]^-$ | −18.6 | $^2[M(N_2)(CO)]^- + e^- \rightarrow {}^3[M(N_2)(CO)]^{2-}$ | 24.0 |
| $^3[M(N_2)(NHC)] + e^- \rightarrow {}^2[M(N_2)(NHC)]^-$ | −1.09 | $^2[M(N_2)(NHC)]^- + e^- \rightarrow {}^3[M(N_2)(NHC)]^{2-}$ | 20.4 |
| $^3[M(N_2)(PMe_3)] + e^- \rightarrow {}^2[M(N_2)(PMe_3)]^-$ | −7.37 | $^2[M(N_2)(PMe_3)]^- + e^- \rightarrow {}^3[M(N_2)(PMe_3)]^{2-}$ | 24.8 |
| $^3[M(N_2)(NH_3)] + e^- \rightarrow {}^2[M(N_2)(NH_3)]^-$ | −7.14 | $^2[M(N_2)(NH_3)]^- + e^- \rightarrow {}^3[M(N_2)(NH_3)]^{2-}$ | 24.2 |
| $^3[M(N_2)(Py)] + e^- \rightarrow {}^2[M(N_2)(Py)]^-$ | −8.54 | $^2[M(N_2)(Py)]^- + e^- \rightarrow {}^3[M(N_2)(Py)]^{2-}$ | 23.2 |
| $^3[M(N_2)(Acn)] + e^- \rightarrow {}^2[M(N_2)(Acn)]^-$ | −9.53 | $^2[M(N_2)(Acn)]^- + e^- \rightarrow {}^3[M(N_2)(Acn)]^{2-}$ | 24.0 |
| $^3[M(NHC)_2] + e^- \rightarrow {}^2[M(NHC)_2]^-$ | 6.03 | $^2[M(NHC)_2]^- + e^- \rightarrow {}^3[M(NHC)_2]^{2-}$ | 33.9 |
| $^3[M(CO)_2] + e^- \rightarrow {}^2[M(CO)_2]^-$ | −19.7 | $^2[M(CO)_2]^- + e^- \rightarrow {}^3[M(CO)_2]^{2-}$ | 29.6 |
| $^3[M(PMe_3)_2] + e^- \rightarrow {}^2[M(PMe_3)_2]^-$ | 3.89 | $^2[M(Pme_3)_2]^- + e^- \rightarrow {}^3[M(PMe_3)_2]^{2-}$ | 35.0 |
| $^3[M(NH_3)_2] + e^- \rightarrow {}^2[M(NH_3)_2]^-$ | 5.23 | $^2[M(NH_3)_2]^- + e^- \rightarrow {}^3[M(NH_3)_2]^{2-}$ | 30.5 |
| $^3[M(Py)_2] + e^- \rightarrow {}^2[M(Py)_2]^-$ | 1.39 | $^2[M(Py)_2]^- + e^- \rightarrow {}^3[M(Py)_2]^{2-}$ | 26.4 |
| $^3[M(Acn)_2] + e^- \rightarrow {}^2[M(Acn)_2]^-$ | 0.07 | $^2[M(Acn)_2]^- + e^- \rightarrow {}^3[M(Acn)_2]^{2-}$ | 29.6 |

tioned. Deprotonated porphyrins are di-anionic, and Scheiner *et al.* calculating it as neutral would account for the discrepancy in the number of electrons. Furthermore, we found three sets of doubly degenerate orbitals which did not match those of Scheiner *et al.*. For example, the lowest degenerate set depicted in figure 3.2, contained one orbital of $e_g$ symmetry whose counterpart had inconsistent symmetry with the $D_{4h}$ point group. Upon comparison with the [Mo(Por)] electron structure, it became evident that this was a linear combination of $e_g$, $a_{2u}$ and $b_{2u}$ orbitals that could easily be identified in the Mo complex. This most likely occurred due to the calculations not employing symmetry adapted orbitals. Using a molecular visualization program (Chemcraft) the orbitals could be summed and subtracted to yield the four parent orbitals shown with dotted lines on figure 3.2, leading to a consistent orbital structure with the calculations of Scheiner *et al.*. The same had occurred with the set sandwiched between the two, however, there was an unusually large energy difference of 108 kcal/mol between it and its matching counterpart, whereas this type of orbital mixing happens more commonly to orbitals of similar energy.

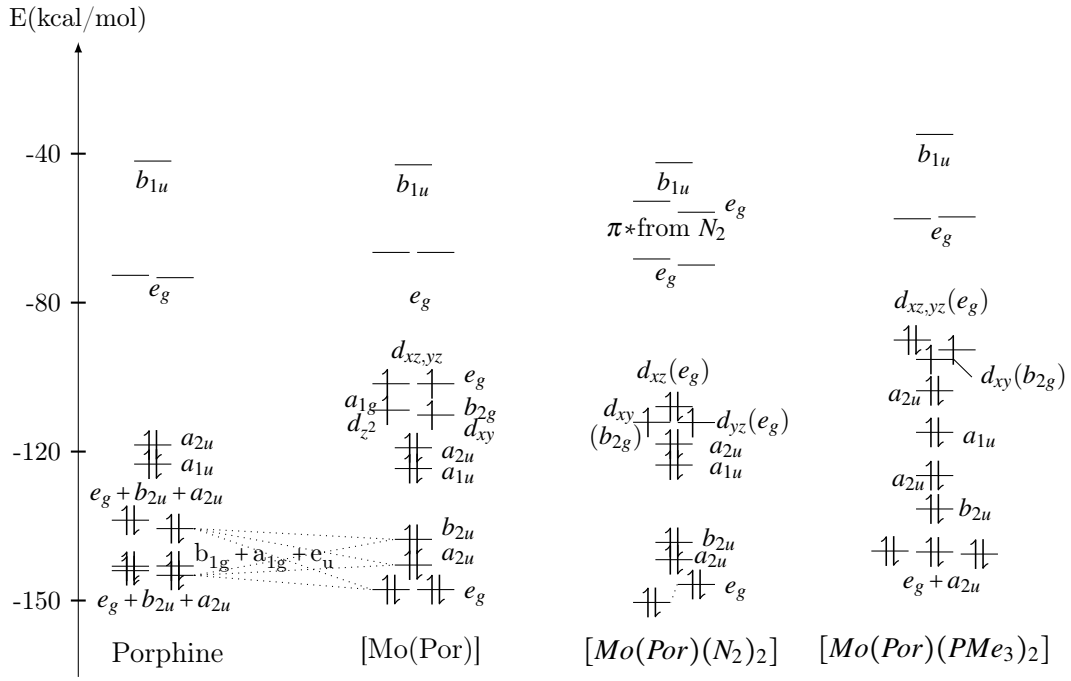


*Figure 3.2: MO diagrams of the selected complexes for study. The metalloporphyrins, having symmetrical axial ligands, share the $D_{4h}$ symmetry of their porphine parent molecule, apart from perhaps the $P(Me)_3$ complex, but same symmetry labels were used for convenience. The orbitals have been symmetry labeled, as have strong metal d-orbital characteristics. This analysis was mainly performed on the $\alpha$ orbitals, and afterwards, $\beta$-orbitals were used to pair up the electrons. Energies are all based on $\alpha$ orbital energies, although it should be noted that severe differences in orbital mixing, and thus energy, of $\alpha$ and $\beta$ was often observed between the two due to spin polarization. Orbitals labeled with sums of symmetry labels were linear combinations of orbitals having those symmetries (see text)*

The square planar porphinatomolybdenum complex has a high spin of S=2. Having no axial ligands, the $d_z^2$ orbital and the $d_{xy}$ are more or less degenerate, affording a stable high spin structure. The triplet state, where one of the $e_g$ electrons is flipped, giving it $\beta$ spin, results in the $e_g$ orbitals losing their degeneracy, and is destabilized by 14 kcal/mol. The singlet state with all electrons paired is further destabilized by an additional 26 kcal/mol. The $b_{1g}$ orbitals of the free base porphine and the $d_{x^2-y^2}$ form bonding and antibonding orbitals outside the energy range of figure 3.2, explaining their absence in the figure. Considerable mixing between

the metal and porphine $e_g$ orbitals was also apparent, the gap between them being 35.5 kcal/mol. Adding one electron, it goes to the metal $e_g$, as opposed to the $a_{1g}$ or $b_{2g}$. It is difficult to say exactly what is taking place, as the order of $\beta$ orbitals in energy differs from that of the $\alpha$, making the $e_g$ orbitals lower in energy than the $a_{1g}$ and $b_{2g}$ (energies on diagram are from $\alpha$ orbitals). The second electron fills the other metal $e_g$ orbital, leaving the complex with two singly occupied orbitals which are lower in energy than the HOMO (using $\alpha$ energies). Both metal and porphine $e_g$ orbitals increase in energy with each reduction, resulting in a slight lowering the gap between them. The presence of a $d_{z^2}$ orbital also explains the relatively low energy in reducing the square planar complex by two electrons compared to the others (see table 3.1 for energies), as the second electron goes to a porphine $e_g$ orbital in the absence of the $d_{z^2}$, which is much higher in energy.

Ligands in the axial position bind through the $a_{1g}$ ($d_{z^2}$) orbital, resulting in bonding and antibonding orbitals with energies outside the scale on figure 3.2, analogous to the $b_{1g}$ orbital of porphine binding to metal. The gap between the metal and porphine $e_g$ orbitals increased by 2.7 kcal/mol. Antibonding $\pi$ orbitals of $N_2$ were 15.5 kcal/mol above the porphine $e_g$ orbitals in energy. Mixing between $e_g$ orbitals of $N_2$, metal and porphine was observed. With only three metal d orbitals left in the HOMO-LUMO region, the triplet state was the most stable, being 9.8 kcal/mol more stable than the singlet state. A similar situation arose where the order of orbital energies was not the same with respect to $\alpha$ and $\beta$ spin resulting in one of the $e_g$ orbitals having paired electrons, and losing their degeneracy as a result. Reduction of one electron leads to both $e_g$ orbitals being doubly occupied and $b_{2g}$ becoming the HOMO, with only 2.1 kcal between the metal $e_g$ and $b_{2g}$ orbitals. All orbitals are raised in energy by $\approx$ 18.8 kcal/mol in the first reduction, with little effect on gaps between them. The second electron surprisingly occupies the $e_g$ orbital of porphine, leaving the system in a singlet state. These results indicate that for some reason the metal $d_{xy}$ orbital is unable to accept a second electron, explaining why one of the $e_g$ orbitals has paired electrons in both six-coordinate complexes in figure 3.2 instead of the $b_{2g}$, furthermore, why an electron would occupy an orbital which is 33.1 kcal higher in energy rather than pairing with the electron in the $b_{2g}$ metal orbital.

In the case of [Mo(Por)($PMe_3$)$_2$], the metal $e_g$ orbitals are higher in energy than the $b_{2g}$ orbitals. Yet again, one of the $e_g$ orbitals has paired electrons, while the other, along with the $b_{2g}$, is singly occupied. The energy of all orbitals was raised substantially compared to the $(N_2)_2$ complex as a result of coordinating to strong $\sigma$ donor ligands, as can be seen on figure 3.2. The $a_{2u}$ porphine orbitals, just below the metal d-orbitals, had a strong interaction with a phosphine orbital

mainly through lobes of the N atoms in the porphine plane, resulting in 3 MOs, the antibonding being the closest to the metal d-orbitals, a non-bonding orbital between $a_{1u}$ and $b_{2u}$ , and a bonding orbital close to the bottom $e_g$ in energy. Unfortunately the same mishap with linear combinations of orbitals happened in the case of the bonding orbital, making it difficult to assign energy to it as the contribution from each orbital to make the linear combination was unknown. Reduction with one electron increased the energy of all orbitals without significant change in gaps between them. As in the case of $N_2$, the first electron fills the other metal $e_g$ orbital, and the second one going to the porphine $e_g$ orbital. Although the energy difference between metal and porphine $e_g$ orbitals is 3.1 kcal/mol lower than in the $(N_2)_2$ comlex, the second reduction step is exothermic by 35.0 kcal/mol compared to only 18.5 in the $(N_2)_2$ complex.

Molybdenum in the planar porphine system can be reduced quite easily to Mo(0), having the $d_{z^2}$ orbital energetically available to accept electrons. In contrast, the second electron reduces porphine in presence of axial ligands regardless of ligand type, which is endothermic of $\approx$ 20 - 35 kcal/mol. The reduction of porphine as opposed to the metal explains why the system reverts to a triplet state upon addition of two electrons. Finally, $N_2$ as a ligand reduces the energy required for the second reduction step to a point where it is thermodynamically allowed at ambient conditions. This may be a result of the mixing between metal, porphine, and $N_2$ orbitals discussed earlier, however, further analysis is needed to say with certainty.

## 3.2. $N_2$ binding and activation

Finding a suitable axial ligand to allow for $N_2$ coordination to molybdenum proved quite challenging. Tuczek *et al.* calculated the free reaction enthalpy change for binding $N_2$ to the Schrock by calculating the difference in energy of the $[HIPTN_3Mo(N_2)]$ complex and the $[HIPTN_3Mo] + N_2$ separated[56]. We felt it was more appropriate to calculate $N_2$ coordination relative to other ligands in our model as the porphinato-molybenum complex appeared to be unstable in its planar form, which presented itself in highly exothermic coordination to almost any axial ligands. Figure 3.3 contains an energy diagram of substitution reactions of various axial ligands, L, with $N_2$. The figure uses $[(Por)Mo(II)L_2]$ as a reference at 0.0 kcal/mol, and shows the energy of substitution with $N_2$, both directly and following a one-electron reduction. As previously stated, all reduction steps discussed in this study are relative to $Cp_2Co$, as it has been used experimentally in catalytic $N_2$ reduction[8,25], see

example in equation3.1.

$$[(\mathrm{Por})\mathrm{Mo}(\mathrm{N_2})_2] + \mathrm{Cp_2Co} \xrightarrow{\Delta \mathrm{E}} [(\mathrm{Por})\mathrm{Mo}(\mathrm{N_2})_2]^- + [\mathrm{Cp_2Co}]^+ \tag{3.1}$$

Calculations predict most ligands to bind more favorably to the metal than $N_2$ does. As can be seen in the figure, only Acn and $NH_3$ can accomodate binding as axial ligands, and only after a primary reduction step. It appears that the ligand of choice for $N_2$ substitution can be neither a very strong $\pi$ acceptor, nor too strong of a $\sigma$ donor. Ligands such as acetonitrile, an easily substituted coordinating solvent, or $NH_3$, a moderate $\sigma$ donor, are the only ones binding more weakly than $N_2$. Pyridine came as a surprise, as it is often described as an equally strong or weaker ligand than $NH_3$, and steric effects were expected to weaken the bonding, nevertheless, it binds slightly more favourably than $NH_3$ and $N_2$. The strong $\sigma$ donors, $PMe_3$ and NHC simply bind too strongly to be substituted for $N_2$. In hindsight we realised that the data for the CO ligand is flawed. The basis sets used in the calculations were smaller for C and H atoms (def2-SVP) than for any other atom (def2-TZVP). Binding of CO to molybdenum through the carbon atom is over-stabilized due to basis set superposition error, meaning the C atom binding to molybdenum steals part of the metal's larger basis set, resulting in an overestimate of binding energy.

Substitution of acetonitrile with $N_2$, having a stronger ligand in the other axial position was also considered, i.e. [(Por)Mo(Acn)L]. In general the most favorable pathway was a reduction of the complex followed by substitution of Acn with $N_2$, with the exeption of fluoride as a ligand where the steps were in reversed order. The results can be found in table 3.2. Basis set superposition error is not an issue here, as there is no substitution of CO. The reaction with CO as the other axial ligand was the only one that showed any improvement from having two Acn ligands in the reaction, with the energy of reduction and substitution about 4 kcal/mol more endothermic. It should also be noted that the reason for omitting flouride in figure 3.3, is that calculating binding energy relative to ionic species with any accuracy is very difficult due to solvent effects.

In order to evaluate whether the system was sensitive to peripheral substitutions with respect to $N_2$ binding, the equatorial plane was systematically changed and the energy of $N_2$ substitution with Acn calculated. Mo(II) complexes of pyridine (py), bipyridine (bipy), terpyridine (tpy), tetraphenylporphyrin (TPP), octaethylporphyrin (OEP) and Phthalocyanine (PCN) were calculated, keeping two Acn

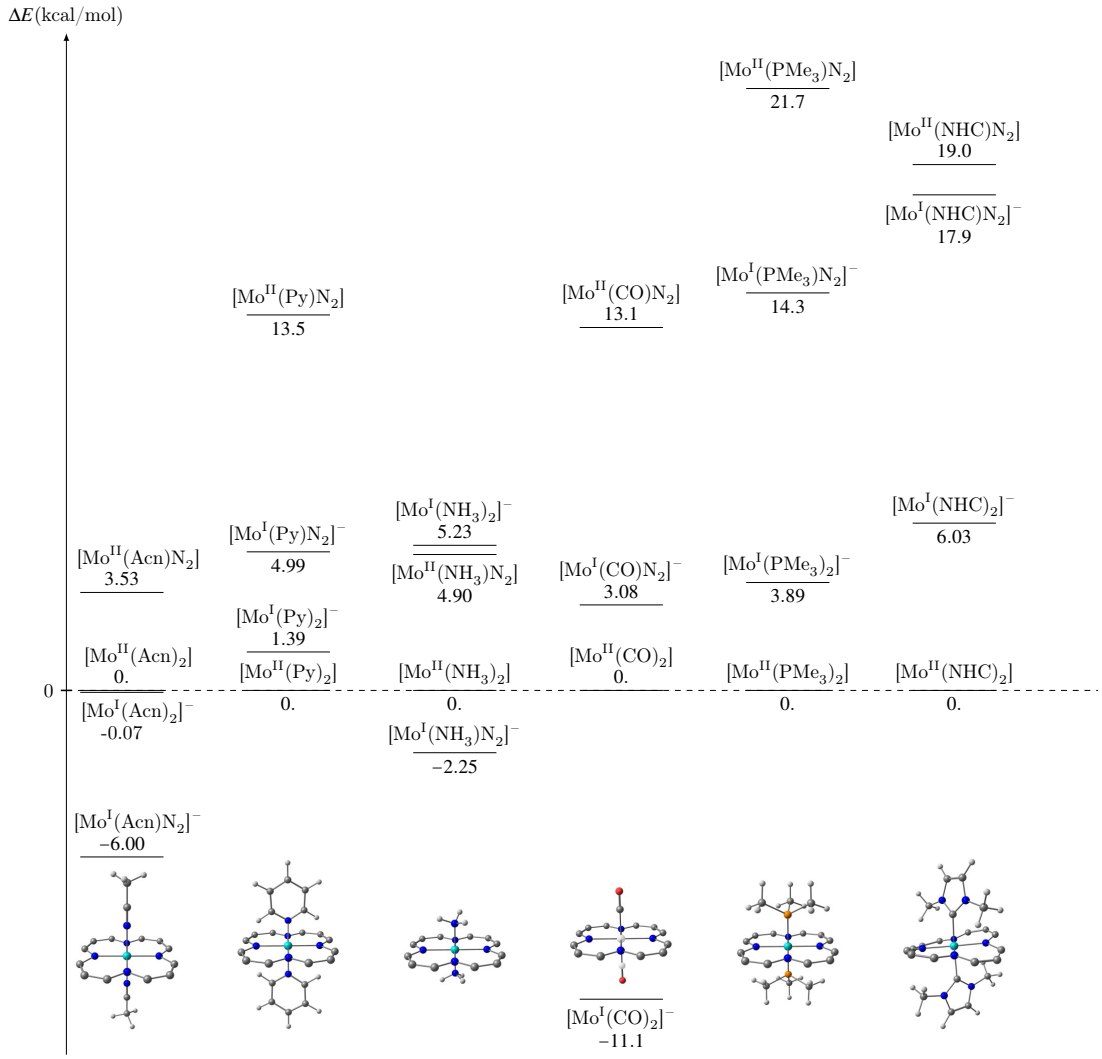


*Figure 3.3: An energy diagram displaying the binding energy of $N_2$ to porphinatomolybdenums with different axial ligands. The [(Por)Mo(II)$L_2$] species have been set to zero energy for reference, from which the relative energy of reduction, with respect to $Cp_2Co$, and $N_2$ substitution with L can be seen. Direct substitutions without reduction are also included in the figure, although they are generally more unfavorable. Pictures of the complexes with simplified porphine structures are at the bottom of the figure, see fig. 3.1 for the complete porphine structure*

ligands in the axial positions. The py complex had four py molecules in the equitorial plane, and the bipy complex two bipy molecules. In the case of tpy, a fourth ligand was needed in the equatorial plane, where py was used. The last

*Table 3.2: A table showing the energy of reduction of [(Por)Mo(II)(Acn)L], and the consequent substitution of Acn with $N_2$. The first entry is a complex with two Acn ligands for comparison. The total charge of the complex is increased by -1 when $L = F^-$*

$$\mathrm{Mo(Acn)L} \xrightarrow[\Delta E_1]{e^-} + [\mathrm{Mo(Acn)L}]^- + \xrightarrow[\Delta E_2]{N_2} [\mathrm{MoN_2L}]^- + \mathrm{Acn}$$

| L | $\Delta E_1$ kcal/mol | $\Delta E_2$ kcal/mol | $\Delta E_{tot}$ kcal/mol |
|---|---|---|---|
| Acn | -0.07 | −5.93 | −6.00 |
| $F^{-*}$ | 9.26 | −8.88 | 0.38 |
| NHC | 2.46 | -0.04 | 2.42 |
| $PMe_3$ | 1.43 | −5.16 | −3.73 |
| Py | 0.38 | −5.57 | −5.19 |
| CO | −11.0 | 0.67 | −10.4 |

* The energies displayed for $F^-$ are for reversed order of steps, i.e. substitution followed by reduction.

three molecules are all common larger porphyrins than porphine, two of which can be seen in figure 1.3, and PCN can be seen in the pictures at the bottom of figure 3.4, where the results may also be found. Binding of $N_2$ occurs through the same basic mechanism for all complexes, which is reduction of the complex followed by a substitution of Acn with $N_2$. The Mo(II) complexes have been given energy of zero as reference points from which the reduction and subsequent substitution can easily be followed above or below on the diagram. As before, reductions are always relative to $Cp_2Co$.

The complexes seem quite sensitive to peripheral substitution, given the results in figure 3.4. However, in order to maintain the same oxidation state of molybdenum in complexes of uncharged ligands (to the left of $[(\mathrm{Por})\mathrm{Mo}(\mathrm{Acn})_2]$), the complexes had to be calculated with a +2 charge, which may give misleading results and account for the exothermic reductions. Nevertheless, looking only to the porphyrins, the ethyl groups of OEP inhibit reduction of the complex, although it still binds $N_2$. In contrast, the larger aromatic system in PCN facilitates reduction of the system leading to a very stable anion, rendering $N_2$ substitution endothermic. The phenyl rings of TPP have little effect as they are twisted out of the molecule's plane and therefore not conjugated to the rest of the system, making TPP behave very similar to porphine with regard to binding $N_2$.

As previously mentioned, Tuczek *et al.* correlated N-N vibrational frequency, both

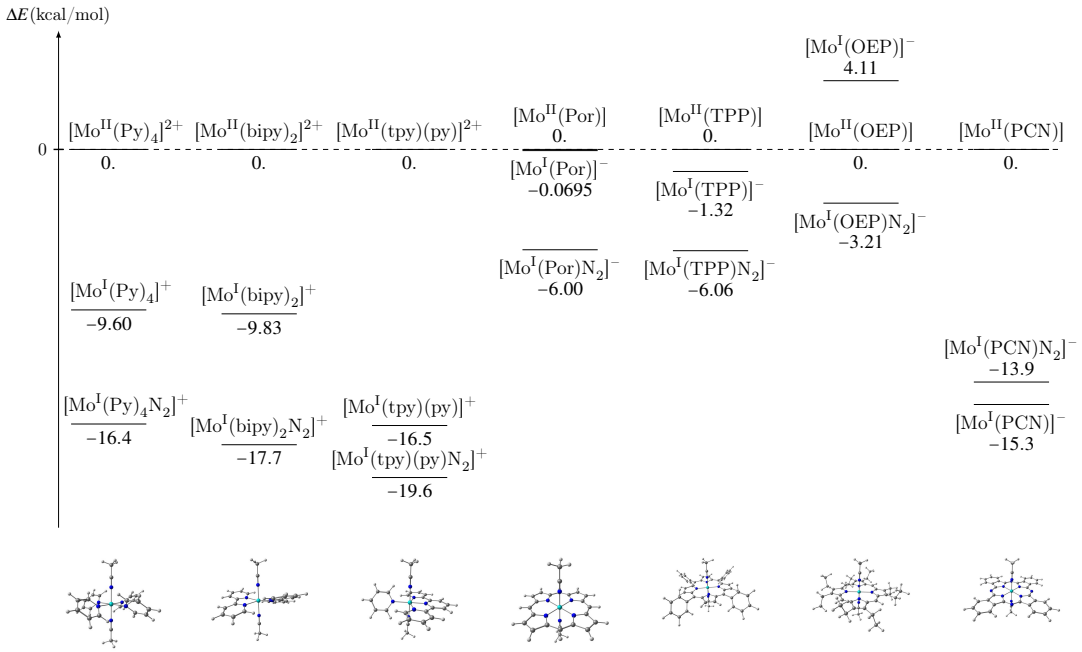


*Figure 3.4: An energy diagram showing the energy of reduction followed by substitution of Acn with $N_2$ in complexes varying in equatorial coordination. Going to the right on the diagram, the delocalized $\pi$ system around the metal increases in size, starting at 4 py molecules and ending with PCN, with [(Por)Mo(acn)$_2$] in the middle for comparison.*

calculated and experimental, as well as calculated NPA charges on the N atoms and N-N bond lengths, with $N_2$ activation[17], i.e. the energy required to protonate $N_2$. We calculated the energy of protonating the $N_2$ substrate in the complexes discussed above with lutidinium acid ($LutH^+$), where the energy of $LutH^+ \longrightarrow Lut + H^+$ is included in every protonation, and compared the required energy to our calculations of the parameters described by Tucek *et al.*. Lutidinium has been used experimentally as a proton source in successful $N_2$ reduction reactions, for example in the work of Schrock *et al.*[8]. It became evident in our calculations that a primary reduction step is necessary for the activation of $N_2$ in the Mo(II) complexes, based on highly endergonic protonations of their $N_2$ substrates, ranging ≈30 - 40 kcal/mol for the ones calculated. Therefore, N-N vibrational frequencies, Hirshfeld charges instead of NPA, and protonation energies were calculated for the Mo(I) species, and are reported in table 3.3. Halogenated complexes also assume higher negative charge, in order to maintain the same oxidation state of molybdenum for comparison to the other complexes.

*Table 3.3: The energy of protonating [(Por)Mo(N2)L] complexes where L are different axial ligands trans to $N_2$. In addition the harmonic vibrational frequency, Hirshfeld atomic charge and bond length of the $N_2$ ligand are included in the table. Charge (Ch.) are calculated Hirshfeld atomic charges, reported for both $\alpha$ (coordinated) and $\beta$ N atoms. When L = halogen, the total charge of the complex is increased by -1*

$$[(Por)Mo(N_2)L]^- \xrightarrow{H^+} + [(Por)Mo(N_2H)L] + \Delta E$$

| Complex | $\Delta E$ kcal/mol | $\tilde{\nu}_{NN}$ $cm^{-1}$ | Ch. $\alpha$ $e^-$ | Ch. $\beta$ $e^-$ | N-N Å |
|---|---|---|---|---|---|
| $[(Por)Mo(Py)N_2]^-$ | 9.23 | 1908.3 | −0.0898 | −0.215 | 1.143 |
| $[(Por)Mo(NH_3)N_2]^-$ | 6.40 | 1879.3 | −0.102 | −0.241 | 1.147 |
| $[(Por)Mo(Acn)N_2]^-$ | 9.33 | 1912.7 | −0.0922 | −0.217 | 1.143 |
| $[(Por)Mo(PMe_3)N_2]^-$ | 9.01 | 1919.8 | −0.0853 | −0.205 | 1.141 |
| $[(Por)Mo(NHC)N_2]^-$ | 7.56 | 1947.5 | −0.0713 | −0.187 | 1.137 |
| $[(Por)Mo(CO)N_2]^-$ | 27.7 | 2069.1 | −0.0298 | -0.096 | 1.178 |
| $[(Por)Mo(N_2)N_2]^-$ | 19.5 | 2036.5 | −0.0131 | −0.141 | 1.133 |
| $[(Por)Mo(Cl)N_2]^{2-}$ | 2.75 | 1854.7 | −0.110 | −0.259 | 1.151 |
| $[(Por)Mo(F)N_2]^{2-}$ | 0.142 | 1850.6 | −0.114 | −0.261 | 1.151 |

Overall the results can be considered exceptionally good compared to the 16.6 kcal/mol required for the first protonation in the most recent calculations of the Schrock cycle[24], or older calculations of the Chatt cycle where the first protonation was endothermic by 21.5 kcal/mol[18], although bearing in mind that those values were free reaction enthalpies, which include thermal, entropic and zero point energy corrections, not included in the calculations reported here. Additionally, we are comparing to calculations performed with the B3LYP functional, while our calculations were performed using the BP86 functional. Atomic charges (especially on the $\beta$ N), bond lengths and vibrational frequencies correlate quite well to the energy of protonation, with the exception of the NHC ligand, where these parameters indicate worse activation than any non-$\pi$ acceptor, yet a rather low energy of protonation.

Strong $\pi$ acceptors are the least activating *trans* ligand, which is unfortunate as the best $N_2$ binding is predicted with CO in the axial position. This was to be expected as a result of the *trans* effect. $N_2$ activation relies on $\pi$ backbonding from the metal, weakening its triple bond, and having another ligand in the *trans* position accepting electrons through $\pi$ backbonding via the same orbital naturally reduces the effect. Strong $\sigma$ donation appears to aid the $N_2$ activation, while at

the same time it may inhibit binding. The halogens, on the other hand, are good $\pi$ donors which appear to lower the energy of protonating $N_2$ significantly, although it may also be an effect of increasing the charge of the complex in order to keep the oxidation state of molybdenum unchanged with halogens as ligands. Moderate $\sigma$ donors like $NH_3$ and Acn. (weaker), are possibly the key to dinitrogen activation according to these calculations, in view of having relatively low first protonation energies, in addition to being suitable ligands for binding of $N_2$ to the complex.

Activation of $N_2$ was also studied with respect to equatorial changes, by calculating the same step and parameters for the complexes from figure 3.4. Unfortunately, data is missing for a few harmonic frequency calculations, N-N frequencies are reported where data existed. Results can be found below in table 3.4.

*Table 3.4: The energy of protonation of various [Mo(Acn)($N_2$)] complexes that differ in the equatorial plane. Complexes of uncharged ligands (non-porphyrins) have a charge of +1 in order to keep the same oxidation state of molybdenum as in the di-anionic porphyrin complexes, which carry a total charge of -1. Protonations are calculated with lutidinium.*

$$[LMo(Acn)N_2]^n \xrightarrow{H^+} + [(L)Mo(Acn)(N_2H)]^{n+1} + \Delta E$$

| Complex | $\Delta E$ kcal/mol | $\tilde{\nu}_{NN}$ $cm^{-1}$ | Ch. $\alpha$ $e^-$ | Ch. $\beta$ $e^-$ | N-N Å |
|---|---|---|---|---|---|
| $[(Acn)Mo(py)_4N_2]^+$ | 15.9 | 1883.7 | −0.113 | −0.253 | 1.153 |
| $[(Acn)Mo(bipy)_2N_2]^+$ | 21.4 | 1919.0 | −0.111 | −0.217 | 1.146 |
| $[(Acn)Mo(tpy)(py)N_2]^+$ | 24.2 | - | −0.0901 | −0.184 | 1.142 |
| $[(Acn)Mo(Por)N_2]^-$ | 9.33 | 1912.7 | −0.0922 | −0.217 | 1.143 |
| $[(Acn)Mo(TPP)N_2]^-$ | −0.482 | - | −0.0893 | −0.208 | 1.142 |
| $[(Acn)Mo(OEP)N_2]^-$ | 5.09 | - | −0.0989 | −0.242 | 1.147 |
| $[(Acn)Mo(PCN)N_2]^-$ | 24.1 | 2023.4 | −0.0520 | −0.120 | 1.131 |

What is probably most striking about the results is how activated $N_2$ is in the pyridine complex. Although the protonation energy is higher than that of porphine, it is not high compared to literature values mentioned above, especially considering that the complex is already positively charged. Furthermore, the low vibrational frequency, and long bond length, suggest a weak N-N bond. Correlation of the calculated parameters to the protonation energy is not as good here as it was in table 3.3. The bipy complex, for example, has the same charge on the $\beta$ N atom as porphine, similar bond lengths, and only a 10 $cm^{-1}$ difference in N-N vibrational frequency, yet the protonation is twice as endothermic. Peripheral substitution of porphyrin rings, clearly has a major impact on its properties and chemical be-

havior. Effects of the substituents of OEP and TPP are more pronounced in the activation than $N_2$ binding, while PCN behaves completely differently from the rest in both cases, displaying virtually no $N_2$ activation. Remarkably, the protonation energy is dramatically reduced in OEP and TPP.

## 3.3. Reaction mechanisms

Acetonitrile and fluoride were chosen as ligands to calculate a minimum free reaction enthalpy pathway ($\Delta G$) towards formation of ammonia. As previously discussed, complexes containing Acn should bind $N_2$ according to our calculations, and was therefore an obvious choice. On the other hand, $F^-$-containing complexes showed great $N_2$ activation and very low protonation energies. The calculated mechanism was loosely based on the Chatt cycle, specifically the one calculated for the complex of tridentate phosphine ligands by Tuczek *et al.*, where more possibilities were explored, rather than the classic Chatt cycle most commonly reported (figure 1.2)[17,19]. Our system, however, behaved quite differently regarding order of steps, and it was consequently decided to explore various combinations of steps, including different spin states, in an effort to map out the energy landscape.

Geometries were optimized with the BP86 functional, using def2-SVP double $\zeta$ basis sets for C and H atoms, and the def2-TZVP triple $\zeta$ basis set for all other atoms. Harmonic frequency calculations were then made with the same functional and basis sets, both to evaluate the N-N vibrational frequency, and to obtain corrections for entropy and zero point energy, allowing for $\Delta G$ calculations. Single point energy calculations using the B3LYP functional and def2-TZVP basis set on all atoms were also carried out. The minimum energy path we have arrived at can be seen in figure 3.5. Preferred spin multiplicities are circled in the top left corner of each intermediate, and total charge is indicated in the top right. In cases where functionals disagreed on lowest energy spin state, both are included. Figures 3.6 and 3.7 show the corresponding energy diagrams, in which the protonation and reduction steps are color coded. Bond orders are, in part, based on the Chatt cycle as well as bond distances and angles from optimized structures.

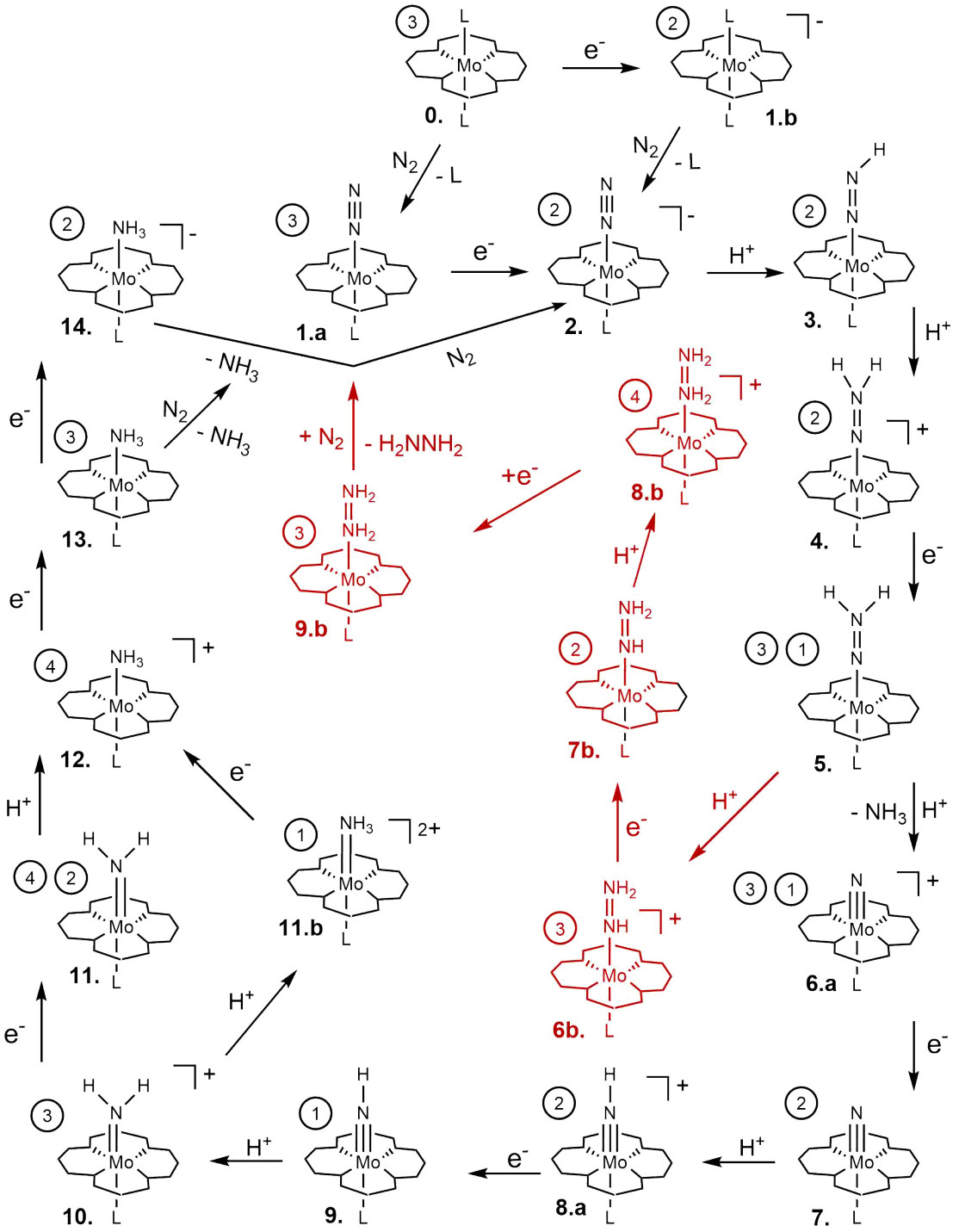


*Figure 3.5: The lowest free reaction enthalpy pathway, as calculated with BP86 and B3LYP, for $NH_3$ formation from $N_2$ reduction using a porphinatomolybdenum catalyst. Spin multiplicities are circled in the top left corner next to each intermediate, and total charge is indicated in the top right corner. A pathway leading to hydrazine formation is colored red. Note that if L = halogen, the total charge is increased by -1 per L.*

In the case of L=Acn, the reaction proceeded through **1b**, as a reduction is needed to achieve $N_2$ binding, while the $F^-$ system was calculated starting from **1a** on the grounds of binding energies calculated relative to negatively charged ligands being unreliable. From **2**, two consecutive protonations yield a complex **4**, a reduced analogue to the hydrazido intermediate, which has been isolated and thoroughly studied by Tuczek *et al.*[17]. In the Chatt cycle, the hydrazido complex is reduced by two electrons yielding a complex analogous to **5**. The two-electron reduction leads to dissociation of the axial ligand, and a triple bond forming between the metal and the coordinated N atom, which will release the first equivalent of ammonia spontaneously upon the next protonation. The axial ligand of **5** did not dissociate in either the $F^-$ or Acn complexes, although the geometry became odd as the $N_2H_2$ ligand started bending, making the M-N-N angle 155° and 153°, possibly due to increased metal N bond order. We tried reducing the complex again and still the axial ligand would not dissociate during optimizatioin, keeping its unusual geometry however. This is subject most definitely warrents further study, considering that if proven energetically favorable, this step may bypass the step leading to hydrazine formation.

Protonation of **5** leads to formation of one equivalent of $NH_3$ being released and a charged Mo-N complex is formed **6a**. The intermediate between **5** and **6.**, not shown here, was calculated and the energy of releasing $NH_3$ was less than 1 kcal/mol. Tuczek *et al.* called his analogue of **6a** a nitrido complex, however, the formation of a nitrido complex is usually the most exergonic step in calculations of catalytic reduction cycles of $N_2$[24], and we did not see such exothermicity until the addition of the next electron (see figures 3.6 3.7), leading us to believe that the triple bond does not form until the electron is added in **7**. Protonation of the nitrido complex yields the imido complex **8**, leading to the amido (**10 11**) and ammine (**11b 12 13**) complexes with alternating steps of protonations and reductions. Intermediate **14.** was originally calculated to be energetically favourable for the Acn system, however, going from **13** to **1a** became the preferred way after adding $\Delta G$ corrections.

The BP86 energy diagrams are remarkable, as they indicate no significant energy barriers in the whole of the cycle. The most endothermic reaction in the cycle for the Acn system is the first protonation, around 8 kcal/mol (10 if you count first 2 protonations). For the $F^-$ system, the most endothermic reactions were the initial reduction and the reduction to form the hydrazido-like intermediate **5**, around 4.1 kcal/mol. In addition it is endothermic of $\approx$ 5kcal/mol to regenerate the catalyst in a substitution of $NH_3$ and $N_2$, including the last reduction to **13** for $F^-$. Interestingly, in the literature, the reduction from **12** to **13** is generally the most

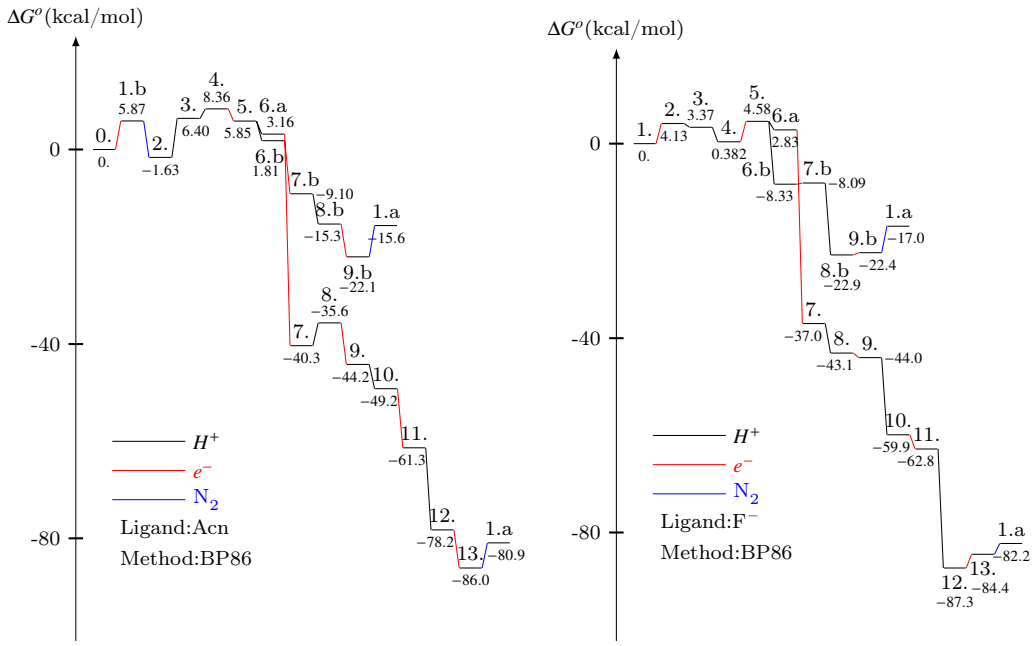


*Figure 3.6: The free reaction enthalpy profile associated with figure 1.2, calculated with BP86 using the def2-SVP basis set for C and H, and def2-TZVP for other atoms. Black lines represent protonation, red lines reductions, and blue lines indicate addition of $N_2$*

endothermic reduction, whereas it is exothermic for the Acn system. Additionally the protonation steps are exothermic for the $F^-$ system, while they are commonly the most endothermic (15 - 25 kcal/mol) in the literature. In both systems the most exothermic step is formation of the nitrido comples, which is quite common in the literature[24,56], however, the reported values of $\Delta G$ commonly range from 60 - 70 kcal/mol, while we calculated them around 30 - 35 kcal/mol. As ideal as all of this sounds for $NH_3$ production, this pathway ultimately prefers hydrazine formation, with steps leading to splitting in the pathway almost equal in energy in the Acn system, and being ≈5 kcal/mol lower in the $F^-$ case. Several pathways toward $NH_3$ formation from the hydrazine pathway were explored and hydrazine formation was always energetically more favorable. However, one was overlooked which was the protonation of the $\beta$ nitrogen of **9b**. Furthermore, a pathway, almost without energy barriers, is perhaps unlikely to be an accurate description of $N_2$ reduction, as reducing the strong dinitrogen triple bond typically takes considerable energy,

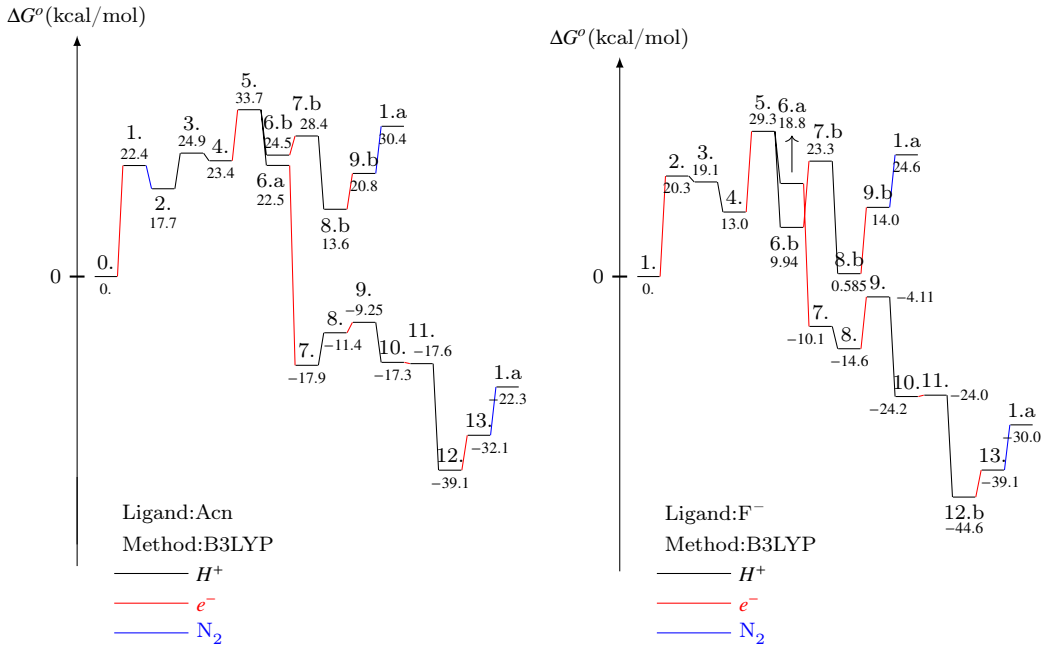


*Figure 3.7: Free reaction enthalpies for the steps in figure 1.2 from singlepoint energy calculations with the B3LYP functional and def2-TZVP basis set for all atoms. Geometries come from BP86 optimizations. Black lines are between protonation steps, red between reduction steps and black where $N_2$ is added.*

seeing that nitrogenase enzymes use 16 equivalents of ATP per $N_2$ and $H_2$[3].

The energy pathway calculated with the B3LYP functional paints a very different picture. The first reduction step has increased from 5 kcal/mol to 20.3 and 22.4 kcal/mol. This is more in the range of literature values for the first protonation, which is commonly the most endergonic step[23,24]. The protonations are still calculated as being exothermic for the $F^-$ system, which renders the reduction to 5. even more endothermic. After formation of the nitrido complex, there is still a bit of an energy barrier of one reduction and protonation to reach the imido complex **9**, which was non existent in the case of $F^-$ in BP86 calculations. Yet another energy barrier in the B3LYP calculations is the energy barrier to regenerate the catalyst, which has increased by ≈10kcal/mol for both systems. The difference between pathways leading to hydrazine has decreased slightly for the $F^-$ system and reversed for the Acn system. Moreover, the final reduction step and regeneration of the catalyst in hydrazine formation has now become 16.8 kcal/mol for the Acn

system and 24 kcal/mol for the $F^-$ system, which suggests that a reaction would likely stop with a build-up of **8b** and **9b** concentration.

Differences in reaction energies calculated by the two functionals most definitely demand further investigation into which functional is describing the system more accurately. Such an investigation would be too large to encompass in this study, however, we did calculate the primary reduction, $N_2$ substitution, and first protonation of the Acn system using the LPNO-pCCSD/2a coupled cluster method, a post HF method which includes determinants of excited states to calculate the correlation energy that HF lacks. After adding thermal and zero point corrections to the results, using the same basis sets as were used in the BP86 calculations. The first reduction step resulted in $\Delta G = 20.7$ kcal/mol, and 5.2 kcal/mol for the $N_2$ substitution, in quite good agreement with the B3LYP values of 22.4 and 4.7 kcal/mol. However, the protonation step was exothermic, going down 8.1 kcal/mol while the B3LYP indicated an endothermic reaction of 7.2 kcal/mol. These results suggest that BP86 is vastly underestimating the energy going into reduction steps, and moreover, perhaps the B3LYP functional is also describing the system poorly regarding protonation steps, emphasizing the need for further study into the subject.

This study has revealed several problems in the Chatt-like reduction cycle of molybdenum metalloporphyrins, the most obvious being the sensitivity of the model with respect to level of theory. The $N_2$ activation and binding study was performed with the, possibly inadequate, BP86 functional, and may need to be repeated with B3LYP or another appropriate functional based on a benchmarking study. Another problem is hydrazine formation. If the unexplored possibility of $NH_3$ formation from the hydrazine pathway leads to a dead end, then adjusting the system with different ligands would be a possible solution, which in itself is a third problem due to the amount of factors that need to be taken into account in such adjustments. The system would have to be able to bind and activate $N_2$, while avoiding the hydrazine pathway, in addition to keeping the $NH_3$ pathway favorable. In spite of the many difficulties, we feel that the results of this study call for a follow-up research.

# 4. Conclusions

Although it is not clear at this point whether B3LYP or BP86 is describing the system more accurately, comparison to other studies, coupled with the fact that nitrogenase uses substantial energy in the reduction of $N_2$, indicate that BP86 is underestimating the energy required for the reduction steps. Yet, these results clearly call for a benchmarking study to establish reliable protocols for describing metalloporphyrins with quantum chemical calculations.

Nevertheless, we do feel that we have shown that metalloporphyrins of molybdenum should achieve considerable activation of $N_2$, given the low protonation energies predicted by both methods employed, in addition to the harmonic vibrational frequencies and Hirshfeld atomic charges calculated on the $N_2$ atoms. In addition, several of the complexes should bind $N_2$, where strong $\sigma$ donor ligand inhibiting $N_2$ binding whilst increasing activation, and strong $\pi$ acceptors decreasing activation, although strong binding could be achieved when using a $\pi$ acceptor in the axial postition if $N_2$ was substituted for a weaker ligand, such as acetonitrile.

Notwithstanding, we have also showed that the parameters commonly used for benchmarking $N_2$ activation, atomic charge of N and harmonic frequencies of N-N bonds, may give misleading results. We found outliers in both directions, i.e. considerable activation with harmonic frequencies and charges suggesting otherwise, as well as low activation with harmonic frequencies and atomic charges suggesting considerable activation. Therefore, protonation energies must be calculated in order to reliably evaluate activation.

Finally, a reaction pathway most likely leading to the formation of hydrazine, was calculated as equally energetically favorable as a path towards $N_2$ formation when using acetonitrile as the axial ligand, and more favorable when fluoride was used. The sensitivity of the system to different axial ligand and peripheral ring substituents indicates that this may be tuned to favor the formation of $N_2$. However, such a task may prove difficult, as the system would have to be adjusted to bind and activate $N_2$ in addition to favoring the correct pathway.

# 5. References


[1] L. E. Apodaca, *US Geological Survey, Mineral Commodity Summaries, January 2016*, 2016.

[2] V. Smil, *Enriching the earth: Fritz Haber, Carl Bosch, and the transformation of world food production*, MIT press, 2004.

[3] B. M. Hoffman, D. R. Dean and L. C. Seefeldt, *Accounts of chemical research*, 2009, **42**, 609–619.

[4] R. R. Eady, *Chemical Reviews*, 1996, **96**, 3013–3030.

[5] B. M. Hoffman, D. Lukoyanov, Z.-Y. Yang, D. R. Dean and L. C. Seefeldt, *Chemical reviews*, 2014, **114**, 4041–4062.

[6] T. Spatzal, M. Aksoyoglu, L. Zhang, S. L. Andrade, E. Schleicher, S. Weber, D. C. Rees and O. Einsle, *Science*, 2011, **334**, 940–940.

[7] K. M. Lancaster, M. Roemelt, P. Ettenhuber, Y. Hu, M. W. Ribbe, F. Neese, U. Bergmann and S. DeBeer, *Science*, 2011, **334**, 974–977.

[8] D. V. Yandulov and R. R. Schrock, *Science*, 2003, **301**, 76–78.

[9] N. G. Connelly and W. E. Geiger, *Chemical Reviews*, 1996, **96**, 877–910.

[10] R. R. Schrock, *Angewandte Chemie International Edition*, 2008, **47**, 5512–5522.

[11] B. Le Guennic, B. Kirchner and M. Reiher, *Chemistry–A European Journal*, 2005, **11**, 7448–7460.

[12] M. Reiher, B. Le Guennic and B. Kirchner, *Inorganic chemistry*, 2005, **44**, 9640–9642.

[13] J. Chatt, J. R. Dilworth and R. L. Richards, *Chemical Reviews*, 1978, **78**, 589–625.

[14] F. Tuczek, K. H. Horn and N. Lehnert, *Coordination chemistry reviews*, 2003, **245**, 107–120.

[15] Y. Nishibayashi, *Inorganic chemistry*, 2015, **54**, 9234–9247.

[16] W. B. Tolman, *Activation of small molecules: organometallic and bioinorganic perspectives*, John Wiley & Sons, 2006, pp. 87–89.

[17] F. Studt and F. Tuczek, *Journal of computational chemistry*, 2006, **27**, 1278–1291.

[18] G. C. Stephan, C. Sivasankar, F. Studt and F. Tuczek, *Chemistry–A European Journal*, 2008, **14**, 644–652.

[19] H. Broda, S. Hinrichsen and F. Tuczek, *Coordination Chemistry Reviews*, 2013, **257**, 587–598.

[20] S. Hinrichsen, H. Broda, C. Gradert, L. Söncksen and F. Tuczek, *Annual Reports Section" A"(Inorganic Chemistry)*, 2012, **108**, 17–47.

[21] C. J. Pickett and J. Talarmin, *Nature*, 1985, **317**, 652–653.

[22] M. Antberg, C. Prengel and L. Dahlenburg, *Inorganic Chemistry*, 1984, **23**, 4170–4174.

[23] F. Neese, *Angewandte Chemie International Edition*, 2006, **45**, 196–199.

[24] W. Thimm, C. Gradert, H. Broda, F. Wennmohs, F. Neese and F. Tuczek, *Inorganic chemistry*, 2015, **54**, 9248–9255.

[25] S. Kuriyama, K. Arashiba, K. Nakajima, H. Tanaka, K. Yoshizawa and Y. Nishibayashi, *Chemical Science*, 2015, **6**, 3940–3951.

[26] K. Arashiba, Y. Miyake and Y. Nishibayashi, *Nature chemistry*, 2011, **3**, 120–125.

[27] J. S. Anderson, J. Rittle and J. C. Peters, *Nature*, 2013, **501**, 84–87.

[28] S. Mathew, A. Yella, P. Gao, R. Humphry-Baker, B. F. Curchod, N. Ashari-Astani, I. Tavernelli, U. Rothlisberger, M. K. Nazeeruddin and M. Grätzel, *Nature chemistry*, 2014, **6**, 242–247.

[29] D. Dolphin, Z. Muljiani, K. Rousseau, D. Borg, J. Fajer and R. Felton, *Annals of the New York Academy of Sciences*, 1973, **206**, 177–200.

[30] J.-H. Chou, M. E. Kosal, H. S. Nalwa, N. A. Rakow and K. S. Suslick, *Urbana*, 2000, **51**, 61801.

[31] T. Mlodnicka, *Journal of molecular catalysis*, 1986, **36**, 205–242.

[32] M. da GH Vicente and K. M. Smith, *Current organic synthesis*, 2014, **11**, 3.

[33] W. R. Scheidt, *Handbook of Porphyrin Science (Volume 24) With Applications to Chemistry, Physics, Materials Science, Engineering, Biology and Medicine*, World Scientific, 2012, pp. 1–179.

[34] J. R. Gispert, *Coordination chemistry*, Wiley-VCH Weinheim, 2008, vol. 483.

[35] L. M. Berreau, V. G. Young Jr and L. K. Woo, *Inorganic Chemistry*, 1995, **34**, 3485–3490.

[36] A. De Cian, J. Colin, M. Schappacher, L. Ricard and R. Weiss, *Journal of the American Chemical Society*, 1981, **103**, 1850–1851.

[37] E. Schrödinger, *Annalen der physik*, 1926, **385**, 437–490.

[38] D. R. Hartree, Mathematical Proceedings of the Cambridge Philosophical Society, 1928, pp. 89–110.

[39] V. Fock, *Zeitschrift für Physik*, 1930, **61**, 126–148.

[40] J. C. Slater, *Physical Review*, 1930, **36**, 57.

[41] P. M. Gill, *Encyclopedia of Computational Chemistry. New York, NY: John Wiley & Sons*, 1998.

[42] E. Fermi, *Rend. Accad. Naz. Lincei*, 1927, **6**, 32.

[43] L. H. Thomas, Mathematical Proceedings of the Cambridge Philosophical Society, 1927, pp. 542–548.

[44] P. A. Dirac, Mathematical Proceedings of the Cambridge Philosophical Society, 1930, pp. 376–385.

[45] P. Hohenberg and W. Kohn, *Physical review*, 1964, **136**, B864.

[46] J. C. Slater, *Physical Review*, 1951, **81**, 385.

[47] W. Kohn and L. J. Sham, *Physical review*, 1965, **140**, A1133.

[48] A. D. Becke, *Physical review A*, 1988, **38**, 3098.

[49] F. Weigend and R. Ahlrichs, *Physical Chemistry Chemical Physics*, 2005, **7**, 3297–3305.

[50] K. Eichkorn, O. Treutler, H. Öhm, M. Häser and R. Ahlrichs, *Chemical physics letters*, 1995, **240**, 283–290.

[51] S. Grimme, *Journal of computational chemistry*, 2004, **25**, 1463–1473.

[52] A. Klamt and G. Schüürmann, *Journal of the Chemical Society, Perkin Transactions 2*, 1993, 799–805.

[53] F. Neese, F. Wennmohs, A. Hansen and U. Becker, *Chemical Physics*, 2009, **356**, 98–109.

[54] F. Neese, *Wiley Interdisciplinary Reviews: Computational Molecular Science*, 2012, **2**, 73–78.

[55] M.-S. Liao and S. Scheiner, *The Journal of chemical physics*, 2002, **117**, 205–219.

[56] F. Studt and F. Tuczek, *Angewandte Chemie International Edition*, 2005, **44**, 5639–5642.

# A. ORCA input files

**Input file for a geometry optimization:**

! BP86 D3BJ def2-SVP def2-SVP/J Opt Normalprint printbasis TightSCF Grid4 FinalGrid5 slowconv NOSOSCF COSMO NPA

%pal nprocs 2 end

%output Print[ P_Basis ] 2 Print[ P_MOs ] 1 Print[ P_Hirshfeld] 1 end

%cosmo SMD true Solvent "ACETONITRILE" end

%scf MaxIter 1000 end

%basis newgto Mo "def2-TZVP" end newgto N "def2-TZVP" end newgto O "def2-TZVP" end end

*xyz 0 3

6 2.561637299 5.193990433 -5.711427558

1 2.561637299 9.404693450 -4.403726659 *

The ! line defines the type of calculation method basis sets etc. This molecule was optimized using the BP86 functional with def2-SVP basis sets and def2-SVP/J basis sets for the RI-J approximation. Opt is the keyword for geometry optimization. COSMO is for the continuum solvation model and NPA prints natural population analysis. The rest in the line are settings for the SCF and others tell ORCA what to print. The block inputs (%) are quite self explanatory, %pal is used for amount of processors to use. %scf used to set maximum scf iterations, %COSMO sets solvent, %basis defines new basis sets on selected atoms. %output selects information to print.

These are then followed by * xyz 0 3 , where 0 is the charge of the system and 3 is the spin multiplicity, a triplet state here. This is finally followed by Cartesian coordinates of the atoms in Å. the first number being the atomic number followed by XYZ coordinates and a * to close the coordinates. To make a harmonic frequency calculation, for example, one would simply add the keyword "freq"

# B. Geometries

**Optimized geometry of [(Por)Mo(II)(Acn)$N_2$]:** Cartesian coordinates in Å

| | | | |
|---|---|---|---|
| C | 0.781871 | 8.092463 | 2.650385 |
| C | 0.894685 | 8.717119 | 3.964462 |
| N | 0.710536 | 7.742482 | 4.933657 |
| C | 0.493004 | 6.531872 | 4.293123 |
| C | 0.535991 | 6.754942 | 2.851557 |
| H | 0.881927 | 8.623521 | 1.695170 |
| H | 0.394796 | 5.973765 | 2.093728 |
| C | 0.019870 | 3.765563 | 6.959441 |
| C | 0.233935 | 5.047170 | 6.331392 |
| N | 0.412510 | 5.997783 | 7.326248 |
| C | 0.328386 | 5.364719 | 8.558059 |
| C | 0.078147 | 3.961392 | 8.332572 |
| H | -0.151129 | 2.822959 | 6.424067 |
| H | -0.036735 | 3.207718 | 9.121974 |
| C | 1.554654 | 12.111812 | 5.704134 |
| C | 1.275458 | 10.713859 | 5.479158 |
| N | 1.163445 | 10.086038 | 6.711431 |
| C | 1.369862 | 11.031471 | 7.705791 |
| C | 1.612845 | 12.307682 | 7.077256 |
| H | 1.695140 | 12.860680 | 4.914309 |
| H | 1.809482 | 13.245508 | 7.612239 |
| C | 0.896789 | 7.972221 | 11.385636 |
| C | 0.737169 | 7.356269 | 10.072280 |
| N | 0.886493 | 8.337378 | 9.103667 |
| C | 1.139234 | 9.541432 | 9.743587 |
| C | 1.143016 | 9.309674 | 11.184433 |
| H | 0.828068 | 7.435318 | 12.340350 |
| H | 1.315782 | 10.085024 | 11.941708 |
| C | 0.272935 | 5.307917 | 4.941306 |
| H | 0.114921 | 4.436685 | 4.288138 |
| C | 0.479207 | 6.002621 | 9.811934 |
| H | 0.386304 | 5.350206 | 10.693051 |
| C | 1.148559 | 10.071526 | 4.224897 |
| H | 1.269960 | 10.718662 | 3.343347 |
| C | 1.355127 | 10.766176 | 9.095494 |
| H | 1.541843 | 11.632028 | 9.748244 |
| Mo | 0.759262 | 8.047193 | 7.019367 |
| C | 3.986015 | 7.446394 | 6.981717 |
| N | 2.843458 | 7.660642 | 6.990742 |
| C | 5.405348 | 7.180002 | 6.968453 |
| H | 5.894913 | 7.784332 | 6.179259 |
| H | 5.582629 | 6.106439 | 6.759131 |
| H | 5.851501 | 7.435081 | 7.950000 |
| N | -2.345651 | 8.626329 | 7.068117 |
| N | -1.237245 | 8.418434 | 7.050133 |

Using a molecular visualization program, the other complexes can be easily built from from this basic one

# C. Figures

Some interesting figures of complexes that either did not have a figure in the thesis or were not mentioned:

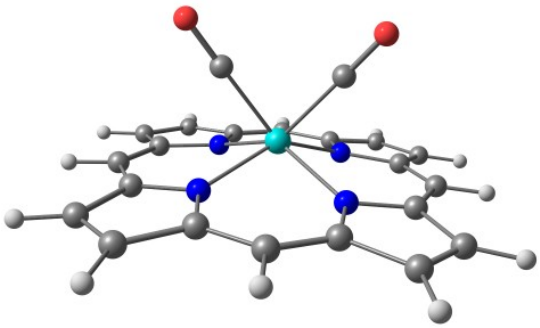

*Figure C.1: The CO complex that has actually been synthesized of a porphinato-molybdenum is cis, and in a singlet state, unlike all complexes we calculated. Unfortunately we did not have access to the article where it was reported, and were not able to get many details.*

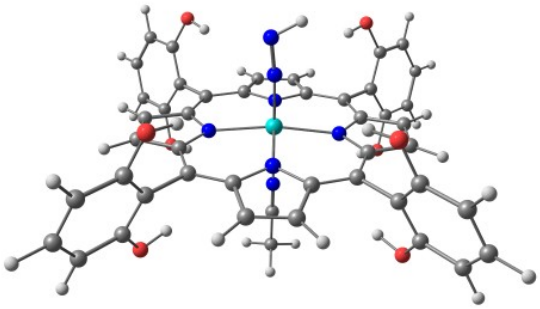

*Figure C.2: A catalyst that was tested for CO reduction, similar to TPP but with 2 OH substituents on each phenyl ring*

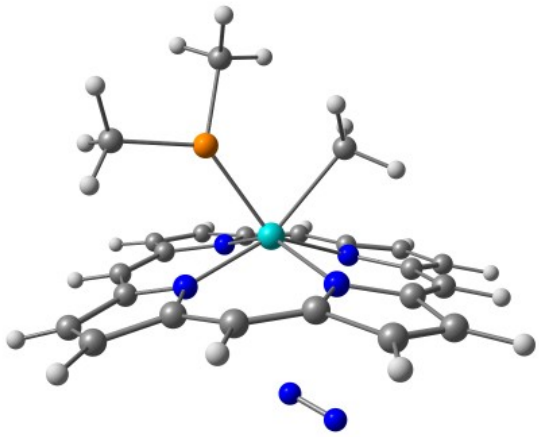

*Figure C.3: This is what happened when trying to calculate the $PMe_3$ complex uncharged in a singlet state*

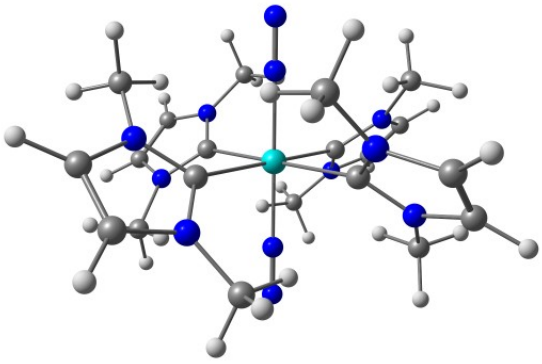

*Figure C.4: A bis(dinitrogen)complex with NHC ligands in the axial plane*